# Investigating an Area of Reduced Wall Thickness as a Mechanism of Abdominal Aortic Aneurysm Initiation

by

Stephanie Gibbons

A Thesis submitted to the

School of Graduate Studies

In partial fulfillment of the requirements for the degree of

**Master of Science**

**Faculty of Medicine**

**Memorial University of Newfoundland and Labrador**

**October 2023**

St. John's Newfoundland and Labrador

**Abstract**

Few previous studies of Abdominal Aortic Aneurysms (AAAs) have incorporated empirical measurements to compare against their corresponding computational material models. Even fewer studies have been conducted to investigate causes of AAAs. The research objective of this thesis is to investigate an area of reduced wall thickness as a factor in aneurysm initiation, using a "tissue-like" material and comparing with the material model most commonly used for aortic simulations. A "tissue-like" silicone material, Smooth-Sil 940, was selected and a study was completed to obtain the characteristics of the material. The material was then utilized to create specimens for a physical experimental model, and its material properties were utilized to generate computational models with the same material characteristics and geometry of the experimental models. Two studies were then completed in parallel; one computational and one experimental. When both studies were completed the results were compared and observations were made regarding the validity of the computational models, and the impact of an area of reduced wall thickness. Results from both studies suggest that an area of reduced wall thickness could be a critical factor for aneurysm initiation.

**Summary**

Abdominal Aortic Aneurysms (AAAs) are often studied using computer modeling. However, very few studies have been completed comparing computer generated results to the results of laboratory testing. Additionality, there are minimal studies available that have investigated the initiation of AAAs. The objective of this thesis is to investigate an area of reduced aortic wall tissue as a potential factor in the creation of AAAs. Laboratory tests were completed using a silicone model to simulate aortic tissue. The silicone was tested to determine the material properties which were used to make computer models with the same characteristics and geometry as the laboratory tested models. The computer models were tested using the same criteria as the laboratory tested silicone models. The results were then compared and observations were made regarding the validity of the computer models, as well as the impact of an area of reduced wall thickness.

**Acknowledgements**

There are many people I need to thank for helping through the challenge of finishing this Master's program. First, I need to thank my main supervisor, Dr. Nakhla. You did so much more than secure additional funding, and provide technical support. You provided support and understanding throughout all the obstacles that were thrown my way both academically and personally. By providing guidance, but also giving me room to learn and research on my own, I believe I have gained many skills that I will now be able to carry to all future endeavours. Thank you for all you have done, without your patience, support, guidance and understanding this work would not be completed. I am extremely grateful for all you have done.

I must thank my other supervisory committee members. Dr. Fraser, I am so incredibly appreciative of how supportive you have been throughout my Master's program. Providing advice and suggestions, allowing me to use space in your lab, and permitting me borrow equipment to complete my testing all had significant impacts on me being able to continue my master's in a timely fashion and I am very appreciative. Dr. Dubrowski, without the funding you secured, the advice you offered, and the workspace you provided early in my program I would not have been able to do this program. Thank you for all you have done.

I also need to thank Dr. Elruby, who was not a part of my committee, but provided me with guidance throughout my degree, especially with respect to my testing. Your support, advice and kindness did not go unnoticed and was appreciated.

Outside of those in the University, I need to thank my family and friends. To my husband, Adam, you provided me with continued support and encouragement throughout my degree. We had the added challenge of bringing our beautiful daughter, Isla, into the world while I was doing my master's and while the whole world was experiencing the COVID-19 pandemic. You never failed to be there when I needed you. Thank you for being 70% on days I only had 30% to give.

To my parents, in-laws, siblings, and friends, without your support of our family over the course of my master's I never could have gotten to this point. In so many ways you all provided the support I needed to finish this program; watching Isla so I could get in a few more hours of work, listening when a week had been challenging, cooking suppers, helping us to have fun when we needed it, the list could go on and on. I will never forget everything you did for me during this time.

I cannot thank you enough,

Stephanie Gibbons

**Table of Contents**

**Abstract** i

**Summary** ii

**Acknowledgements** iii

**Table of Contents** v

**List of Figures** viii

**List of Tables** x

**List of Abbreviations** xi

**Chapter 1 Introduction** 1

1.1 Research Objective 1

1.2 Thesis Outline 1

1.3 Novelty and Importance of Work 2

1.4 Co-authorship Statement 3

**Chapter 2 Literature Review** 4

2.1 Overview of the Cardiovascular System 4

2.1.1 Vessel Structure 4

2.1.2 Arterial System 7

2.1.3 Capillaries 8

2.1.4 Venous System 8

2.2 Blood Flow and Pressure 8

2.3 Aorta 9

2.4 Abdominal Aortic Aneurysms 13

2.4.1 Treatment 13

2.5 Initiation of Abdominal Aortic Aneurysms 14

2.5.1 Reduction in Aortic Wall Thickness 17

2.5.2 Atherosclerotic Disease and Remodelling 17

2.5.3 Other Potential Factors 18

2.5.4 Increased Aortic Wall Thickness 18

2.5.5 Computational Study of Abdominal Aortic Aneurysm Initiation 19

2.6 Silicone as a "Tissue-like" Material and Experimental Testing 20

2.7 Computational Models of Abdominal Aortic Aneurysms 22

Chapter 3 Material Characterization of a Tissue-like Polymer 24

3.1 Material and Mechanical Testing 24

3.1.1 Material and Specimen Preparation 25

3.1.2 Testing Procedures 29

3.2 Material Model 31

3.3 Hyperelastic Model 32

3.4 Linearly Elastic Model 33

3.5 Results and Discussion 34

3.6 Limitations 42

3.7 Conclusions 42

Chapter 4 Investigating an Area of Reduced Wall Thickness as a Mechanism for Abdominal Aortic Aneurysm Initiation Using Commonly Used Computational Material Models and "Tissue-like" Material. 44

4.1 Computational Studies - Finite Element Analysis 45

4.1.1 Model Geometry 45

4.1.2 Material Models 47

4.1.3 Mesh Convergence 49

4.1.4 Computational Pressure Testing 52

4.2 Experimental Testing 54

4.2.1 Specimen Fabrication 54

4.2.2 Experimental Test Set-up 59

4.2.3 Experimental Pressure Testing 63

4.3 Results and Discussion 64

4.4 Limitations 78

4.5 Conclusions 79

Chapter 5 : Summary 81

References 84

**List of Figures**

Figure 2.1 Circulatory System.....6

Figure 2.2 Anatomy of the aorta and auxiliary arteries .....11

Figure 2.3 Micrographs of stained aortic tissue .....12

Figure 2.4 Micrograph of an EvG Stained sample from a stage 1 AAA. .....16

Figure 3.1 Sheet Mold for Fabricating Silicone Sheets .....26

Figure 3.2 Manufactured specimen die cutter and associated profile geometry .....27

Figure 3.3 Silicone tensile test specimen .....28

Figure 3.4 Silicone specimen in INSTRON E10000 .....30

Figure 3.5 Stress-strain curves for (a) 1.5mm and (b) 3mm Specimens.....35

Figure 3.6 Mean stress-strain curves for 1.5mm and 3mm specimen tests.....36

Figure 3.7 Stress-strain curves (a) a 1.5 mm specimen and (b) a healthy human aortic tissue.....37

Figure 4.1 Geometry for computational and experimental models. .....46

Figure 4.2 Measurement location for mesh convergence studies.....50

Figure 4.3 Mesh convergence studies completed for each computational model.....51

Figure 4.4 Applied boundary conditions and internal loading. .....53

Figure 4.5 Initial mold design for silicone tube specimens.....56

Figure 4.6 Final mold design for silicone tube specimens. .....57

Figure 4.7 Resulting tube specimen from (a) 3D printed mold (b) aluminum mold.....58

Figure 4.8 Set-up of tube specimens during experimental testing.....61

Figure 4.9 Experimental test set-up for pressure testing silicone tube specimens .....62

Figure 4.10 Change in Radius due to applied Internal Pressure.....68

Figure 4.11 Change in Diameter with Internal Pressure for strains less than 1.089.....71

Figure 4.12 Location along the length where radial deformation was measured. ..... 73

Figure 4.13 Change in radius along length for both the hyperelastic computational model and experimental models ..... 74

Figure 4.14 Hyperelastic computational model with area of reduced wall thickness subjected to 140 mmHg. ..... 76

Figure 4.15 Frame of a pressure test with a reduced wall thickness silicone model at 0 mmHg and 140 mmHg ..... 77

**List of Tables**

Table 2.1 Vessel Wall Characteristics .....7

Table 3.1 Values used to determine strain associated with recommended aneurysm intervention diameter of 55 mm ..... 40

Table 3.2 Best fit hyperelastic constants for uniaxial tensile tests of 1.5 mm and 3 mm specimens ..... 40

Table 3.3 Mean values of hyperelastic material constants for both 1.5mm and 3mm specimens. SD represents the standard deviation..... 40

Table 3.4 Linearly Elastic Material Properties. SD represents the standard deviation ..... 41

Table 4.1 Material properties for Smooth-Sil 940 obtained from uniaxial tensile testing. Details of tensile testing are in Chapter 3 ..... 48

Table 4.4.2 Average values and standard deviations (SD) of tube specimen wall thickness from laser scan ..... 55

Table 4.3 Results of experimental and computational pressure testing. SD represents the standard deviation for the experimental tests. ..... 65

Table 4.4.4 True Strains for Hyperelastic Computational Models ..... 70

**List of Abbreviations**

AAA – Abdominal Aortic Aneurysm

BPA – Blood Pressure Analyzer

CFD – Computational Fluid Dynamics

EVAR – Endovascular Aneurysm Repair

FEA – Finite Element Analysis

FSI – Fluid Structure Interactions

SD – Standard Deviation

SEF – Strain Energy Function

# Chapter 1 Introduction

## 1.1 Research Objective

The research objective of this thesis is to investigate an area of reduced wall thickness as a factor in abdominal aortic aneurysm (AAA) initiation, using a "tissue-like" material and comparing with the material model most commonly used for aortic simulations. This was accomplished in two main parts. This first part consisted of characterizing a molded silicone "tissue-like" material to determine the materials properties. The second part utilized the characterized silicone material to create experimental models and computational models. Both the experimental models and computational models were pressure tested and their results compared to determine the agreement between the experimental and computational models. Observations were also made regarding the possibility of areas of reduced wall thickness contributing to the initiation of AAA.

## 1.2 Thesis Outline

The present thesis is organized into five chapters including this introduction. Chapter 2 provides a detailed literature review that provides background for the material selection and insight into the material models often used for aortic simulations. Chapter 3 details the material characterization of a "tissue-like" material, from tensile testing to data analysis. Chapter 4 uses both the "tissue-like" material as well as its obtained material characteristics to create experimental and computational models. The results obtained from each set of tests were then compared and observations were made. Chapter 5 is a summary of the work completed in this thesis and details proposed future directions to build on the presented studies.

## 1.3 Novelty and Importance of Work

There are very few existing studies completed that compare the most commonly used computational models for aortic simulations to empirical results; Specifically, few previous studies have employed an *in vitro* replica of the computer simulation with empirically derived material properties to investigate causes for AAA initiation. Investigating simplified *in vitro* replicas of computational models is important to ensure that the computational models in question are providing reasonably realistic results to those that would be experienced *in vivo*.

Presently, clinical treatment of AAAs is primarily reactionary, with most AAAs being found inadvertently, as many AAAs are asymptomatic until rupture and few countries currently conduct screening programs [1]–[3]. As a result AAAs are often found when they are already well developed and are left to be monitored until they reach a size of 5.5 cm at which time intervention is often recommended [3]–[6]. Researching potential mechanisms for AAA initiation, such as an area of reduced wall thickness, has the potential to uncover mechanisms that could be used to improve preventative care for those at risk of developing AAAs. Investigating new or under developed mechanisms for AAA formation, such as wall thinning, can provide insight into additional or alternative ways to monitor or treat vulnerable populations for AAAs. Improved understanding of AAA initiation mechanisms could provide new and improved measures of preventative care for those who are susceptible to forming AAAs.

## 1.4 Co-authorship Statement

In this thesis there are 5 contributors; Stephanie Gibbons, Ahmed Elruby, Sam Nakhla, Adam Dubrowski and Graham Fraser. Stephanie Gibbons: methodology, validation, formal analysis, investigation, data curation, original writing drafts, and draft review and editing for all chapters. Ahmed Elruby: methodology, validation, formal analysis, investigation, data curation, and draft review. Sam Nakhla: conceptualization, methodology, validation, formal analysis, investigation, resources, draft review, supervision, project administration, and funding acquisition. Adam Dubrowski: funding acquisition for all chapters. Graham Fraser: investigation and resources for chapter three. [7]

# Chapter 2 Literature Review

This chapter provides the relevant background information to adequately understand the chapters that follow. To understand the implications of AAAs, details are provided on the cardiovascular system, the aorta, and treatments options when a AAA is developed. Potential factors into the initiation of AAAs will be discussed and relevant existing research will be highlighted. This includes computational studies that have been completed investigating AAAs and AAA initiation. Background for the use of silicone as a tissue-like substance and how it has previously been utilized for in vitro testing will also be provided. This information should provide a well-rounded understanding of relevant literature.

## 2.1 Overview of the Cardiovascular System

The cardiovascular system comprises the heart, arteries, arterioles, capillaries, venules and veins. Commonly, the cardiovascular system is viewed as having two vascular circuits, made up of the pulmonary circulation system and the systemic circulation system[8]. The left side of the heart provides blood to the systemic vasculature, which distributes blood through the arterial tree to all organs and is returned via the venous circulation to the right side of the heart. The right side of the heart pumps blood to the lungs to be reoxygenated which is then returned to the left side of the heart[8]. The circulatory system is composed of the arterial system, capillaries, and the venous system (Fig 2.1).

### 2.1.1 Vessel Structure

The structure of blood vessels varies throughout the body to aid in facilitating their role in the cardiovascular system. Arteries and veins are typically composed of three layers; the intima (inner most layer), media (middle layer), and adventitia (outer most layer). The composition of

these layers differs for different vessels. Table 2.1 highlights the general composition differences of these layers for different vessel types. Veins are generally larger in diameter than arteries, with thinner vessel walls given that venous blood pressure is relatively low.

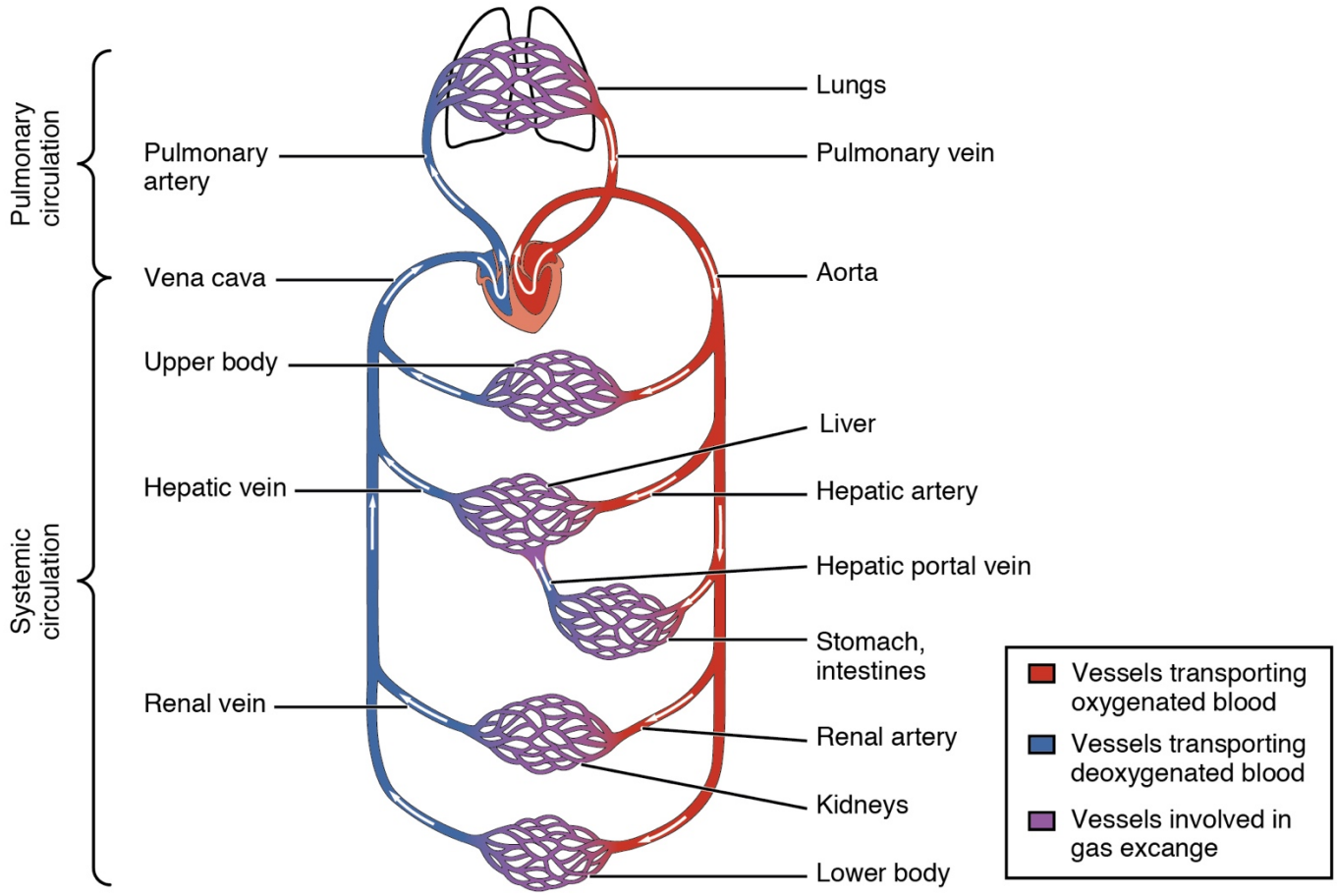


**Figure 2.1 Circulatory System**

[9]

The arterial system takes oxygenated blood from the left side of the heart and distributes it throughout the body, the deoxygenated blood goes to the venous system where it is brought to the right side of the heart

**Table 2.1 Vessel Wall Characteristics**

| | Arteries | Veins |
|---|---|---|
| Intima | Contains internal elastic membrane in larger vessels. Wavy endothelium layer [9]. | No internal elastic membrane. Smooth endothelium [10]. |
| Media | Thickest layer. External elastic membrane. Composed primarily of smooth muscle and elastic fibers (the proportions of each vary depending on the function of the artery) [10]. | Predominately composed of smooth muscle and collagen fibers. No external elastic membrane [10]. |
| Adventitia | Composed primarily of collagen and elastic fibers [10]. | Thickest layer. Composed of collagen and smooth muscle fibers [10]. |

### 2.1.2 Arterial System

The arterial system handles the high-pressure side of the circulation system and is comprised of arteries and arterioles. Arteries can vary in their composition. Elastic arteries, such as the aorta, often have larger radii and are composed of more elastic tissue in their tunica media, allowing them to expand more freely to absorbing and regulating high pressures caused by blood ejection from the heart [11]. Whereas muscular arteries have smaller radii with more smooth muscle tissue in their tunica media, branching to an individual organ [11]. Arterioles conduct blood flow to the capillaries, they have the smallest radii in the arterial system, and due to their small diameters, present the substantial resistance to blood flow. The resistance in individual vessel segments is regulated by the smooth muscle layer(s) located in the tunica media of the arterioles

[11]. Several different factors can contribute to the vasoconstriction and vasodilation of the arterioles that control resistance, such as local factors (ie. myogenic autoregulation), humoral factors (ie. Nitric oxide), and neural factors (ie. The sympathetic nervous system) [11]. These regulatory factors will have some impact on the material properties of the vessel wall, however an in-depth analysis of these factors is beyond the scope of the work completed in this thesis.

### 2.1.3 Capillaries

The capillaries are very small, thin vessels that are arranged in branching networks to facilitate delivery of nutrients, removal of metabolites, and to maintain balance fluids between intravascular and interstitial fluids throughout the body [11].

### 2.1.4 Venous System

Blood is delivered to the venules from the capillaries (or in some cases directly from the arterioles through metarterioles) and is then delivered to the veins to be transported back to the heart [12]. Veins have thinner walls with more elastin and less smooth muscle than arteries, as a result they have a higher compliance than arteries. This means that veins will distend more with less pressure. This allows for higher volumes of blood to be stored in the venous system at lower pressure before returning to the heart.

## 2.2 Blood Flow and Pressure

Blood pressure is the force exerted by blood onto the vessel wall. Blood pressure changes as it makes it way throughout the circulation system. Arteries experience a pulsatile flow of blood due to the systolic (contraction and ejection) and diastolic phases (relaxation and filling) of the

heart [12]. During diastole a bolus of blood is ejected from the left ventricle. As a result, arteries distend significantly to accommodate the influx of blood with each heart beat and experience a sudden increase in blood pressure, then slowly recoil dampening the pulse wave[12]. The pressure pulse wave is further dampened and overall mean pressure further reduced by the arterioles as they provide resistance to flow, and regulate blood distribution. When blood reaches the capillaries there is no longer a pulsatile fluctuation in the blood pressure observed, and the blood pressure continues to decrease along the vascular tree. Blood pressure is at its lowest in the venous system. Venules and veins expand easily to store blood without experiencing a high blood pressure.

The blood pressure experienced in the arterial system varies from person to person. Normal blood pressure is indicated to be 120 mmHg for systolic pressure, and 80 mmHg for diastolic. However, those experiencing high blood pressures can experience systolic pressures exceeding 120 mmHg. In the event of high blood pressure it is recommended that a systolic below 140 mmHg be maintained, with systolic pressures exceeding 140 mmHg requiring intervention [12].

## 2.3 Aorta

The aorta (Fig 2.2) runs from the left ventricle and continues to the bifurcation of the iliac arteries. The section of the aorta that is considered the abdominal aorta begins at the aortic hiatus of the diaphragm and extends downward toward the iliac arteries within the pelvis [13].

The aorta plays a significant role in the flow of blood throughout the circulation system. During systole, the bolus of blood pumped out of the heart causes the aorta to distend under the resulting systolic pressure, due to its elastic nature. Approximately 50% of the blood that is

pumped into the aorta is directed into the rest of the systemic circulation system, while the remaining 50% transiently distends the aorta. During diastole the aorta slowly recoils, pushing the remaining blood volume into the system circulation system. This is referred to at the aorta's windkessel function[14]. This function is a large contributor to the continuous blood flow in the systemic circulation system.

The aorta is the largest of the arteries in the body. As elsewhere in the vascular tree, the walls of the aorta are composed of three layers: the tunica intima, the tunica media, and the tunica adventitia. In the abdominal aorta the tunica media, or medial layer, is generally the thickest layer. The medial layer of the aorta is predominately composed of elastic fibers. The elasticity of the medial layer significantly contributes to the windkessel function [15] .A study by Niestrawska et al [16] focused on how the aortic wall remodels as a AAA develops. The proportion of the layers in the aortic wall in this study was 20:49:31 (intima:media:adventitia). Figure 2.3 shows micrographs from this study of healthy aortic wall tissue. The layers of the aortic wall are clearly visible in this figure, with the heavy presence of elastic fibers highlighted in the media.

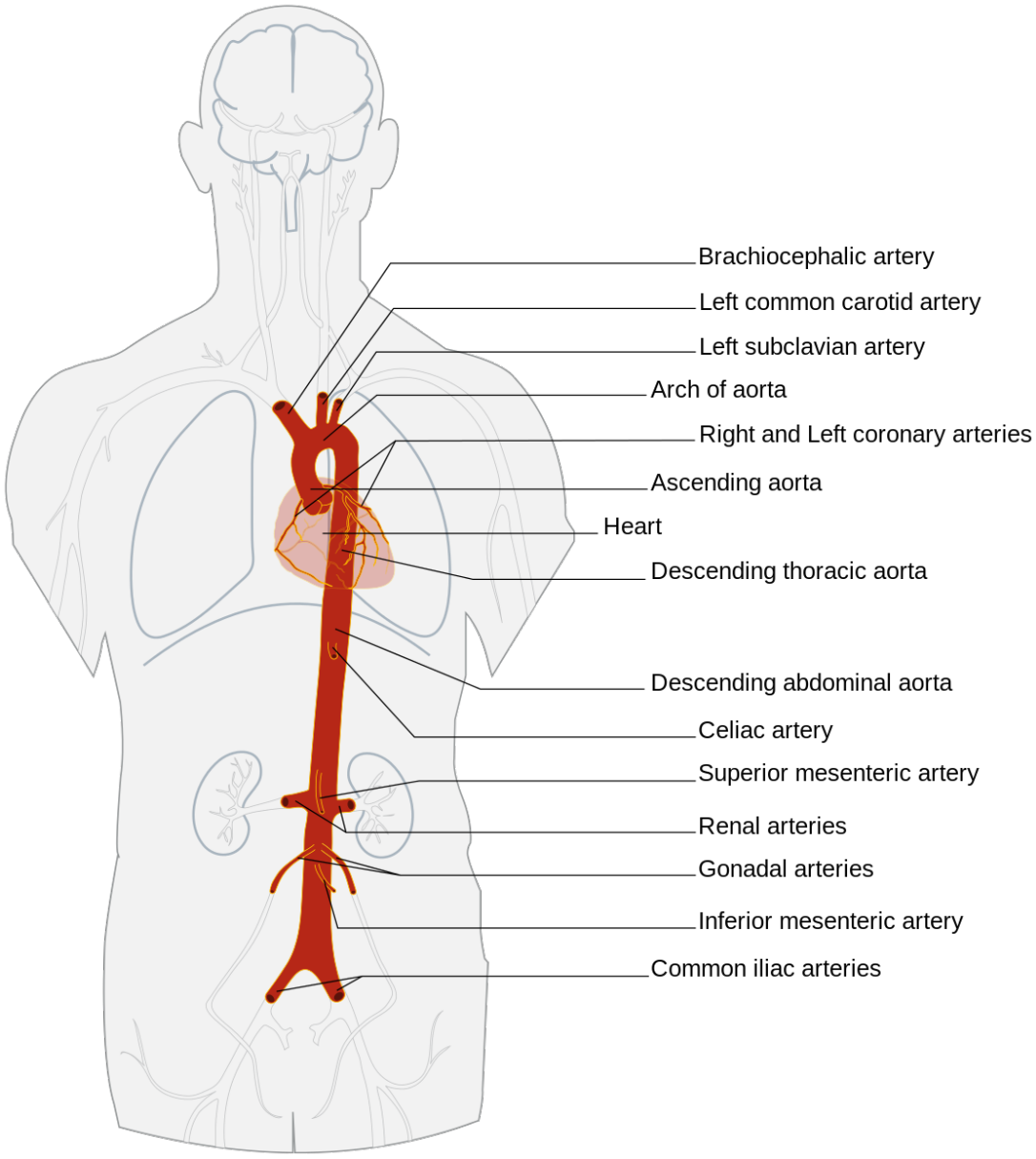


**Figure 2.2 Anatomy of the aorta and auxiliary arteries**

[17]

The aorta is shown in the figure in red, this figure illustrates the aorta heart to the common iliac arteries. Significant auxiliary arteries are also shown.

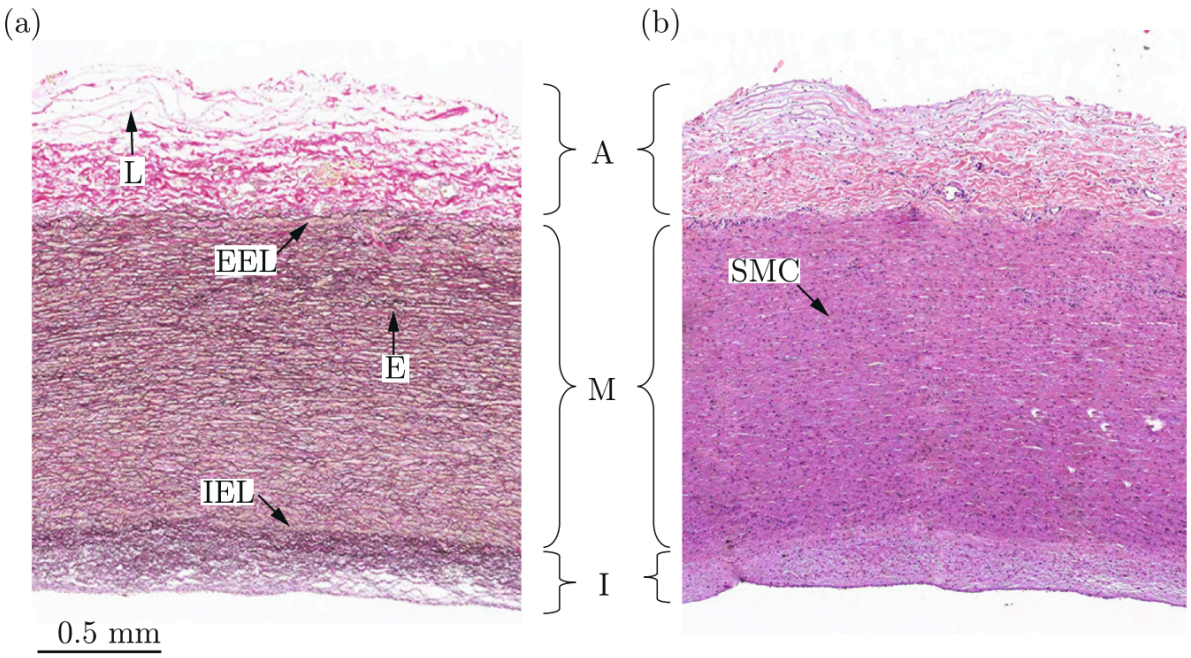


**Figure 2.3 Micrographs of stained aortic tissue**

Images reprinted from The role of tissue remodeling in mechanics and pathogenesis of abdominal aortic aneurysms, Vol 88, Author(s), Justyna A. Niestrawska,Peter Regitnig,Christian Viertler,Tina U. Cohnert,Anju R. Babu,Gerhard A. Holzapfel, Page 5, Copyright 2022, with permission from Elsevier and Copyright Clearance Center.

(a) Strained using Elastica van Gieson (EvG) staining (b) stained using hematoxylin and eosin (H&E) staining. These micrographs clearly show the tissue layers (I = intima, M = media, A = adventitia). Additionally the EvG stained sample allows you to see the internal elastic lamina (IEL), external elastic lamina (EEL), and elastin bundles (E), where as the H&E stained sample allows you to see the smooth muscle cells present in the media [16]

## 2.4 Abdominal Aortic Aneurysms

Abdominal aortic aneurysm (AAAs) are often classified as the aortic segment inferior the renal arteries where the diameter is 30mm or more [2]. AAAs occur where there is a weakening in the arterial wall causing dilations that generally increases over time [18]. In the event of a rupture the mortality rate has been reported to be as high as 65-90%. [2], [3], [19] This is particularly concerning as AAAs are very often asymptomatic prior to the event of a rupture [19]. Many AAAs are undiscovered and those which are discovered tend to be incidental during medical imagining of the abdomen, such as ultrasounds, or through screening programs for at risk populations (ie. smokers, those with familial history, older age) [1]–[3]. Of the known population who develop AAAs, it has been documented that the prevalence increases with age and is more common in males [3]. Previous literature has shown prevalence in women to be 0.7-1% compared to 3.9-4.3% in men. [4], [20].

### 2.4.1 Treatment

Due to many AAAs being discovered inadvertently, the first step to effective treatment of AAAs in the population would be to complete routine screening. A set of guidelines published by the European Society for Vascular Surgery[5] outline that there is evidence to suggest complete screening, preferably using computed tomography angiography (CTA), is beneficial for older men. The same study also suggests that further research completing screening in men and women who have ever smoked, or have a family history of AAAs, may be beneficial.

Historically the decision for elective repair is recommended when the AAA reaches a diameter of 5.5 cm or greater [3]–[6]. This is because current evidence indicates that there is a

significant increase in rupture risk when a AAA expands from 5cm to 6cm [21]. For known non-ruptured AAAs there are 2 options for repair, an open surgical repair or an endovascular repair (EVAR). An open surgical repair involves a laparotomy, or retroperitoneal approach during which the aneurysmal section of the aorta is removed and replaced with a synthetic graft [22]. An endovascular repair is a less invasive approach where a stent graft is inserted to the affected section of aorta through the femoral artery [22]. Endovascular repairs, when possible, are often the preferred approach. A review of unruptured and repaired AAAs documented that endovascular repairs reduced the 30 day all-cause mortality rate when compared to open repairs, and fewer AAA related deaths in the mid-term [23]. However, the same review also noted that reintervention has been reported to be 2-3 times more frequent in patients who have undergone endovascular repair compared to open repair. These findings highlight how important it is to develop treatment plans that can be used for preventative care. Reducing the incidence of AAAs prior to initiation would aid in reducing poor outcomes in fully developed AAA, including ruptures and complications relating to intervention. This can be accomplished by investigating potential mechanisms for AAA initiation. These mechanisms can then be further investigated to determine ways to reduce their occurrence and/or prevent their progression into a AAA.

### 2.5 Initiation of Abdominal Aortic Aneurysms

It has been suggested that most AAAs are non-specific in origin [18]. However, it is generally agreed upon that AAAs form in an area where the vessel wall has weakened. There are a number of known risk factors for the development of AAAs such as smoking, older age, genetics, and male sex [2]. However, the risk factors themselves are not the cause of the AAA formation, but rather they may be contributing factors. Much is still unknown regarding the different causes for aneurysm initiation, however there are a number of theories regarding specific causes of a

AAA. It is believed that in some cases an AAA is attributed to "destruction of elastin and collagen in the media and adventitia" [24]. Niestrawska et al [16] highlighted that in the beginning stage of AAA development there is significant degradation of elastin and remodelling within the wall. Figure 2.4 clearly illustrates a reduction in the medial layer, and elastic fibers at the beginning of aneurysm development comparative to that of the healthy aortic tissue seen in Figure 2.3 with the elastin content decreasing from 20% to only 3% [16]. It also highlights an increase in the intima with the ratio of the layers altered to 40:30:30 (intima:media:adventitia).

This contributes to the hypothesis that the initial cause of an aneurysm could be due to an areas of reduced wall thickness, or a reduction in the medial layer that provides the majority of the elastin in the vessel.

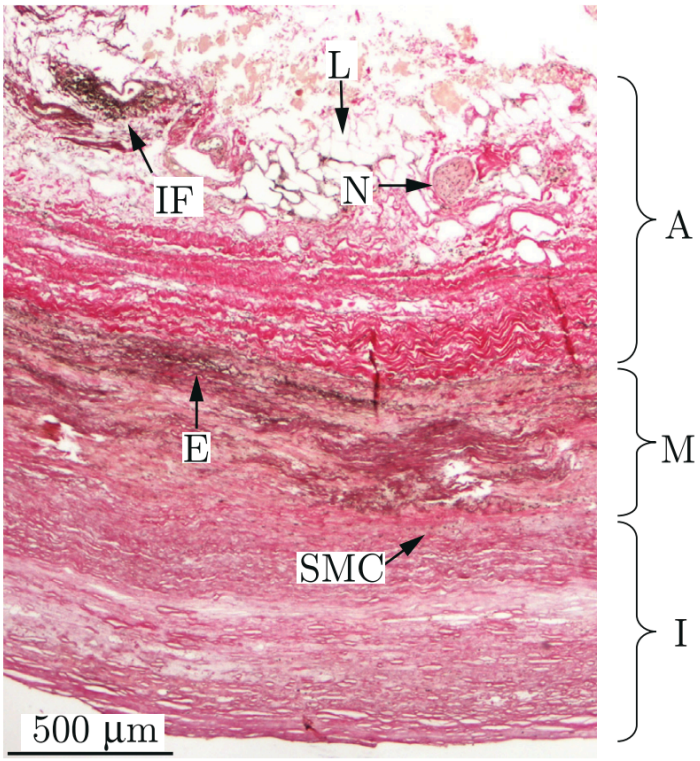


**Figure 2.4 Micrograph of an EvG Stained sample from a stage 1 AAA.**

Image reprinted from The role of tissue remodeling in mechanics and pathogenesis of abdominal aortic aneurysms, Vol 88, Author(s), Justyna A. Niestrawska,Peter Regitnig,Christian Viertler,Tina U. Cohnert,Anju R. Babu,Gerhard A. Holzapfel, Page 6, Copyright 2022, with permission from Elsevier and Copyright Clearance Center.

Compared to the healthy samples, a clear reduction in the thickness of media (M) is present, with increased thickness to both the adventitia (A) and intima (I). There is also a reduction in the visible elastin fibers, and the presence of inflammatory cells (IF). This illustrates the significant remodeling that occurs during AAA formation [16]

### 2.5.1 Reduction in Aortic Wall Thickness

One of the initiating causes of weakening in the vessel walls could be a region of reduced wall thickness, relative to that of the rest of the vessel segment. A study of the thoracic aorta showed that some aortic aneurysm specimens exhibited a reduced wall thickness [25]. It has also been shown that in the area of a AAA the wall thickness is considerably reduced comparative to the rest of the aorta [26]. This study helped raise the salient question: Could a region of reduced wall thickness be the underlying cause of aneurysm initiation?

### 2.5.2 Atherosclerotic Disease and Remodelling

Atherosclerotic disease, or atherosclerosis, is the progressive accumulation of lipids and fibrous elements, most commonly seen in large arteries [27]. Atherosclerotic disease primarily effects the intima and media layers of the vessel wall. Initially the intima is the layer primarily effected, however as the disease progresses the medial layer becomes progressively more involved with smooth muscle cells migrating from the media to the intima [28].

Previously it was thought that AAAs were a direct result of atherosclerotic disease as many patients with AAAs also have atherosclerotic disease [29]. In areas of atherosclerotic plaque build-up in the abdominal aorta it has been reported that the underlying medial layer experiences significant thinning when compared to healthy aortic tissue [30]. A study [31] into expansive remodelling due to atherosclerotic plaque build-up, considered if expansion of the vessel is expansive remodelling or, if it is aneurysm formation. This study acknowledged that labelling the expansion as either expansive remodelling, or aneurysm formation, is often based on the

designation and scope or the research. It also suggests better understanding of medial layer degeneration is required to determine if there is any difference between expansive remodelling or aneurysm formation. However, it is also suggested that AAAs may develop independently of atherosclerotic disease, as not all patients with an AAA have atherosclerotic disease [2].

### 2.5.3 Other Potential Factors

It has been documented that ageing of the human aorta results in fracturing and thinning of the elastic lamellae within the medial layer [15]. In a theory brought forth by O'Rourke [32], he suggested that the thinning experienced by the elastin in the medial layer is a result of fatigue failure. This would be directly related to the pulsatile flow and fluctuating blood pressures experienced by the aorta across the cardiac cycle. The constant pulsating would cause a cyclic stress on the tissue which could cause fatigue and fracturing of the elastic as it responds to the constant change. This theory was supported by the authors *in vitro* testing [33] which showed that the arterial elastin of pigs experiences fatigue failure when subjected to cyclic loading.

### 2.5.4 Increased Aortic Wall Thickness

Studies [34], [35] have shown an increase in wall thickness in abdominal aortic aneurysms. However, the increased wall thickness is thought to be due to a combination of remodelling and inflammatory infiltration which occurs as the aneurysm grows [35]. Remodelling is the ability of arteries to adapt to the effect of arterial disease by increasing wall thickness and composition to maintain adequate flow [36]. As the elastic lamellae fractures and thins in the medial layer, the aorta dilates. The resulting mechanical forces initiates remodelling of the wall with an increase in

collagen in the intimal layer thereby increasing the wall thickness to compensate for the reduction in elasticity [15]. This is thought to be a normal process of aging, as humans age it has been documented that the amount of elastic tissue in arteries is reduced and the wall thickness increased by increased collagen [37].

So, despite the observed increase in wall thickness in full developed AAAs, the possibility of the origin of the aneurysm being an area of the reduced wall thickness cannot be eliminated. Instead, it is possible that the reduction in the thickness, or possibly the loss of elastic properties in the medial layer simulating the effect of medial thinning of the wall may occur first, and remodelling of the arterial wall may be a consequence of the reduced wall thickness, or the subsequent distention. From this perspective it is plausible that an AAA could begin to form in an area where the elastic tissue in the aortic wall has decreased, before remodelling of the wall has had the opportunity to compensate for the loss.

### 2.5.5 Computational Study of Abdominal Aortic Aneurysm Initiation

To date there has only been one computational investigation [38] into abdominal aortic aneurysm initiation. This previous study used a computational model with a 3-layer wall. There were four vessel models that were given "degeneration zones". These degeneration zones were regions of reduced material properties within the medial layer. They created each of these models with both elastic and hyperelastic material models.

Simsek and Kwon concluded from their study that the material properties of the degeneration zones impacted the stress distribution through the three layers of the vessel wall. The

study then evaluated how the distribution of a number of stress and strain values through the vessel wall were affected by the applied degeneration zones. Radial strain through the wall appeared to be primarily unaffected by the introduction of degeneration zones. However, the von Mises stress (a type of stress used to predict yielding of a material under loading) was significantly affected with the medial layer seeing a decrease in stress and the intimal and adventitia layers seeing an increase. The longitudinal strain, radial stress, and radial strain also seemed to be affected by the addition of a degeneration zone, with variations observed based on the applied material models.

They conclude that the use of a hyperelastic material model would be most realistic and should be used going forward. It is also noted in this study that due to the fact there was very little literature available to aid in selecting the most appropriate material properties for these degeneration regions, they suggest that more experimental data is required. Further research is also required to better understand the initiation mechanisms of an aneurysm as it pertains to a reduction in material properties.

### 2.6 Silicone as a "Tissue-like" Material and Experimental Testing

A "tissue-like" material that could mimic aortic tissue was required to complete the forth coming studies. A number of previous studies [39]–[48] have used silicone as a "tissue-like" material when considering soft tissue or a vessel. Though the use of a homogenous material such as silicone is not anatomically accurate due to the layered nature of vessel walls, a homogenous material could be used as a starting point for a simplified approximation. A silicone material has been utilized previously in an experimental model [44] to validate the results obtained from 3D ultrasound speckle tracking. The authors chose silicone as a material comparable to aortic tissue

do validate their 3D ultrasound speckle tracking system due to its similar compliance. Silicone has also been used for its similar compliance and feel for task trainers for medical professionals [40], [42].

In the work completed by Doyle et al. [45], [47], [49] silicone was used to create fully developed aneurysm models for experimental testing. Similar to the current study, they compared the results of the experimental testing to computational models. One such study [45] worked on combining silicones. This was accomplished by using two existing silicones, Sylgard 160 and 170, to create 9 additional silicones by combining the two silicone and adjusting the ratios by 10%, to end with a total of 11 silicones including the Sylgard 160 and 170. Each silicone is characterized and used in a mold of an aortic aneurysm to create a model. The material characteristics were used in a computational model using the Ogden material model, and then all silicone models were pressure tested and compared to experimental results. This approach is similar to the study presented in chapter 4 of the current thesis, however there are some key differences. First, the study by Doyle et al. focuses on fully developed aneurysms of a constant wall thickness. In comparison, the present thesis considers aneurysm initiation using a simplified model with an area of reduced wall thickness. Second, the silicone used in the study completed by Doyle et al. has a higher elastic modulus (2-4 MPa) and the models have a thicker wall (2mm), to correspond with wall thickness values reported for fully developed AAAs as opposed to pre-aneurysmal aortas. This results in a considerably less compliant model, as compliance is the ability of a vessel to respond to increased pressure where,

$$C = \frac{\Delta V}{\Delta P} \tag{1.1}$$

Where C is compliance, $\Delta V$ is the change in volume and $\Delta P$ is the change in pressure. The higher the elastic modulus of a material, the less compliant the material will be, resulting in less deformation. Lastly, Doyle et al. completed automated curve fitting to the closest material model match for their specific silicone. This resulted in the use of the Ogden material model. The current study focuses on utilizing the most commonly employed reduced polynomial material model proposed by Raghavan et al. [50] by following the same process to obtain the material characteristics.

## 2.7 Computational Models of Abdominal Aortic Aneurysms

Due to the nature and complexity of AAAs, computational studies are often completed. Each study tends to focus on one of three areas; computational fluid dynamics (CFD)[51]–[57], finite element analysis (FEA)[58]–[67], or fluid structure interactions (FSI)[38], [68]–[76]. CFD is used to analyze the fluid flow in a defined system, FEA is used to analyze the potential physical reaction of a structural model under specific conditions, such as applied load or pressure, and FSI is often used to study both fluid flow and how the fluid flow effects a structural model.

Additionally, models for aortic aneurysms are often idealized and simplified using linearly elastic or hyperelastic material models. A linearly elastic material produces a stress-strain curve that is linear. A hyperelastic material produces a stress-strain curve that is non-linear. For linear elastic models, a variety of elastic moduli and Poisson's ratios have been used due to the variations reported in human aortic tissue.[68], [70], [75]–[78] Raghavan et al [50] completed a study in

which a reduced polynomial hyperelastic material model, Eq 1.2, was proposed for the aortic aneurysm computational models.

$$W = C_{10}(I_B - 3) + C_{20}(I_B - 3)^2 \quad (1.2)$$

where $W$ is the strain energy density, $I_B$ is the first invariant of the left Cauchy-Green tensor, and $C_{10}$, $C_{20}$ are the parameters for the material properties of their specimens. Raghavan et al. also proposed the hyperelastic constants for the reduced polynomial model. These constants were obtained from analyzing the data acquired from tensile testing aortic tissue that was published by Raghavan et al.[79] The constants were obtained using the constitutive equation, Eq 1.3, also proposed in a subsequent study[50] by the same group.

$$T_1 = \left[2C_{10} + 4C_{20}\left({\lambda_1}^2 + 2{\lambda_1}^{-1} - 3\right)\right]\left[{\lambda_1}^2 - {\lambda_1}^{-1}\right] \quad (1.3)$$

where $T_1$ is traction, and $\lambda_1$ is stretch ratio. The proposed strain energy function and corresponding constants have been utilized in a wide variety of computational studies investigating AAAs. [11], [31], [34], [35], [37], [38], [40], [44], [45], [47], [52]–[57] The vast majority of these studies focus on fully developed aneurysms and are seek to investigate the potential risk of rupture using either FEA or FSI.

# Chapter 3 Material Characterization of a Tissue-like Polymer

In order to characterize the material properties of silicone as the selected "tissue-like" material, uniaxial tensile tests were completed on a number of silicone specimens. The material was determined to be adequately "tissue-like", with respect to aortic tissue, if the specimens exhibited a similar stress-strain response to that of healthy aortic tissue. These sample specimens were fabricated in two different thicknesses to evaluate how the thickness of the specimen would affect the resulting hyperelastic material constants. This chapter details the methods used to create and test the samples, the analysis completed on the resulting data, the results of the testing, and any observations or conclusions drawn.

## 3.1 Material and Mechanical Testing

To complete tensile testing, test specimens needed to be fabricated. For improved translatability, test specimens would be fabricated using a "tissue-like" material, such as silicone. The process of creating the silicone specimens included selecting a specific silicone material, fabrication of a sheet mold, and fabrication of a die cutter to cut out the specimens. After preparing the testing specimens, tensile testing was completed. The following sections outline the preparation of the material and specimens, as well as the details of the tensile tests. The resulting data from the material testing is then utilized to determine hyperelastic and linearly elastic material properties. The hyperelastic and material properties are required to complete further computational analysis.

### 3.1.1 Material and Specimen Preparation

For this study Smooth-Sil 940 silicone (Smooth-On, Macungie) was used. This silicone was selected as the elastic modulus of 1.3 MPa at 100% modulus reported in material data sheet [86] fell within the expected range of elastic moduli for the abdominal aorta [87]. As mentioned previously, it was unknown whether the hyperelastic properties of silicone would vary with different material thicknesses. ASTM D412 recommends a specimen thickness of 3 mm ± 0.3 mm for tensile testing, however for future models a thinner wall thickness will be used. To address this 1.5 mm and 3 mm thick silicone sheets were constructed using sheet molds (Fig. 3.1). After following the measuring and mixing instructions outlined by the manufacturer [86], including time under vacuum to ensure all air bubbles were removed from the mixture, the silicone was poured into the sheet molds and placed under even weighted pressure. These silicone sheets were left to cure for a minimum of 24 hours at room temperature before removal from their molds. Once the silicone sheets were fully cured and removed from their molds. To create silicone specimens for uniaxial tensile testing, an aluminum specimen die was created for this study (Fig. 3.2). The cutter was machined from solid aluminum using a VH-3 Computerized numerical control (CNC) machine (HAAS, Oxnard). The die cutter was created to ensure consistency between specimens, and to reduce the risk of the specimens breaking in an unintended location (anywhere other than the mid-section of the specimen). The dimensions for the specimen die are shown in Figure 3.2. After the fabrication of the die cutter was completed, it was used with a hand press (Dake, Grand Haven) on the silicone sheets to create the silicone specimens (Fig. 3.3).

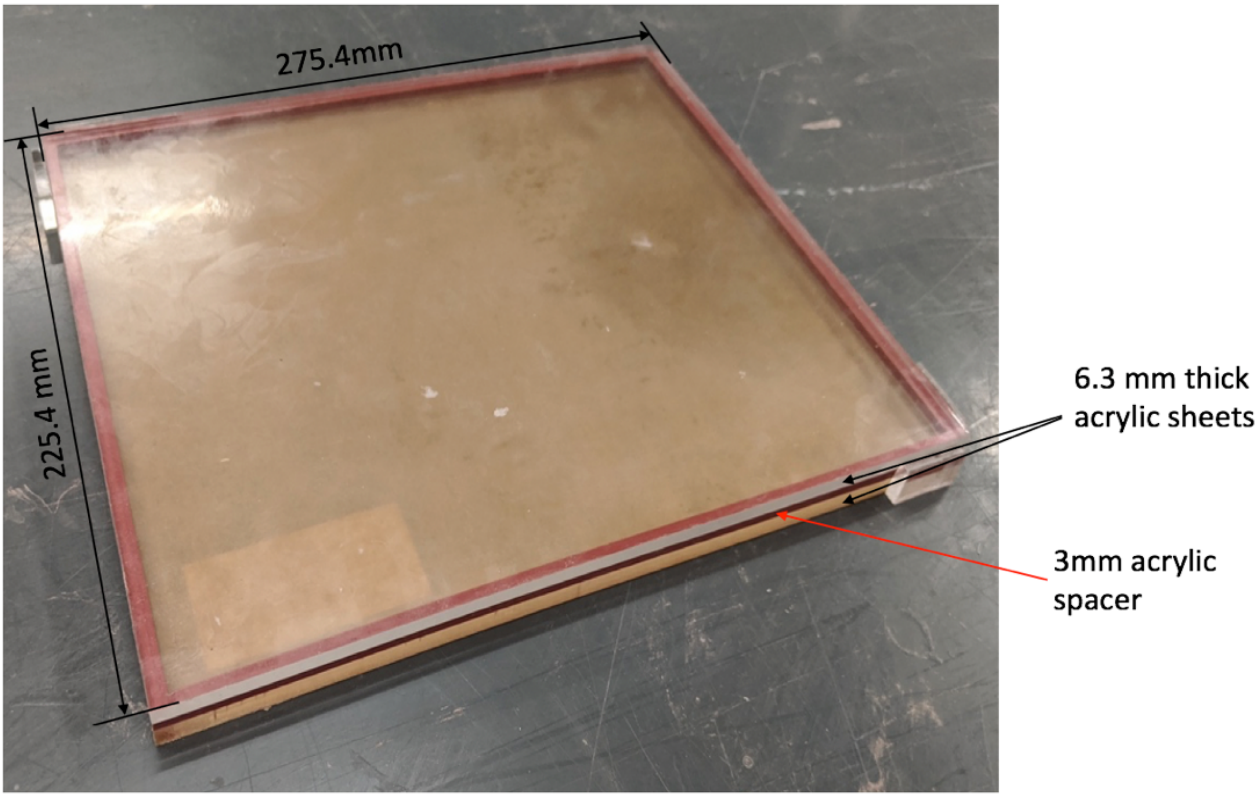


**Figure 3.1 Sheet Mold for Fabricating Silicone Sheets**

Two sheet molds were fabricated for creating silicone sheets. A 1.5 mm mold was fabricated using 6.3 mm acrylic sheets for the base and cover, with a 1.5 mm aluminum spacer. The 3 mm mold was fabricated using 6.3 mm acrylic sheets for the base and cover, with a 3mm acrylic spacer. Both sheet molds have external dimensions of 275.4 mm x 225.4 mm and internal dimensions, which are the dimensions of the resulting cured silicone sheet, of 250 mm x 200 mm.

(a)

(b)

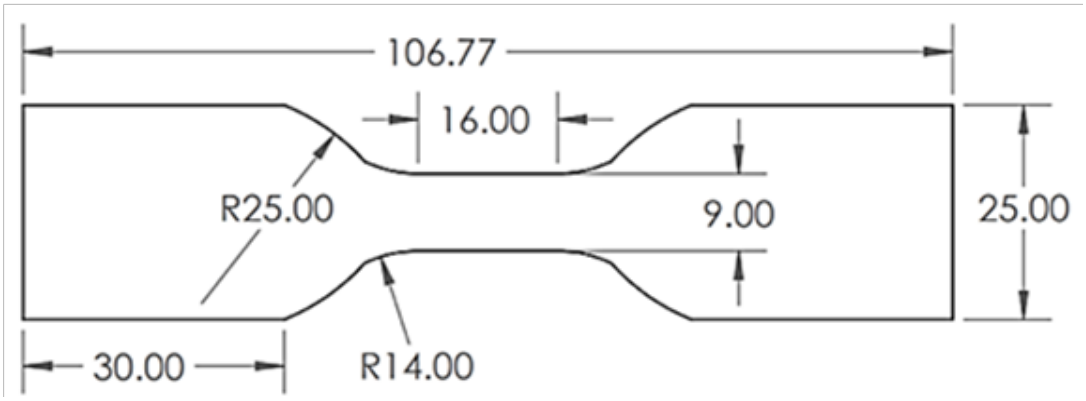


**Figure 3.2 Manufactured specimen die cutter and associated profile geometry**

(a) Manufactured specimen die cutter for cutting silicone specimens to be used in tensile tests (b) Associated profile geometry of silicone tensile test specimens (dimensions provided in mm). The size of the end tabs, as well as the length, of the specimens were specifically chosen to accommodate the testing machine available on site for tensile testing, INSTRON E10000 (INSTRON, Norwood). The end tabs of the specimens were designed to reflect the size of the grips on the tensile testing machine, this allowed for most accurate alignment.

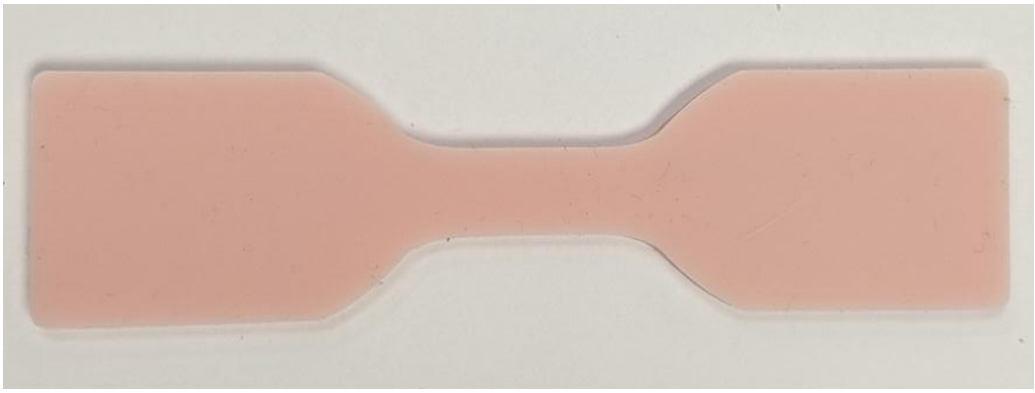

**Figure 3.3 Silicone tensile test specimen**

Resulting silicone specimens from using die cutter with a hand press on silicone sheets. Silicone specimens are to be used in tensile testing.

### 3.1.2 Testing Procedures

Tests for this study were completed using the INSTRON E10000. This machine is equipped with a load cell and a digital image correlation (DIC) video extensometer. The video extensometer allows for the recording of axial and transverse strains as the specimen was stretched. Preceding testing, the thickness of each specimen was checked in 3 locations along the straight narrow section in the middle of the specimen; the average thickness recorded was entered into the testing machine for calculation purposes. Upon inputting the recorded specimen thickness into the testing machine, the silicone specimen was installed in the pneumatic clamps (Fig 3.4). Each test was run at a rate of 8mm/s for a stroke of 58 mm. The grip separation rate of 8 mm/s was chosen as it aligns with the recommendations outlined in ASTM D412 [88]. This process was completed five times for both the 1.5 mm and 3 mm thick specimens for a total of 10 tests. The purpose of testing specimens of two different thicknesses was to observe the potential impact specimen thickness may have on the hyperelastic properties of the material.

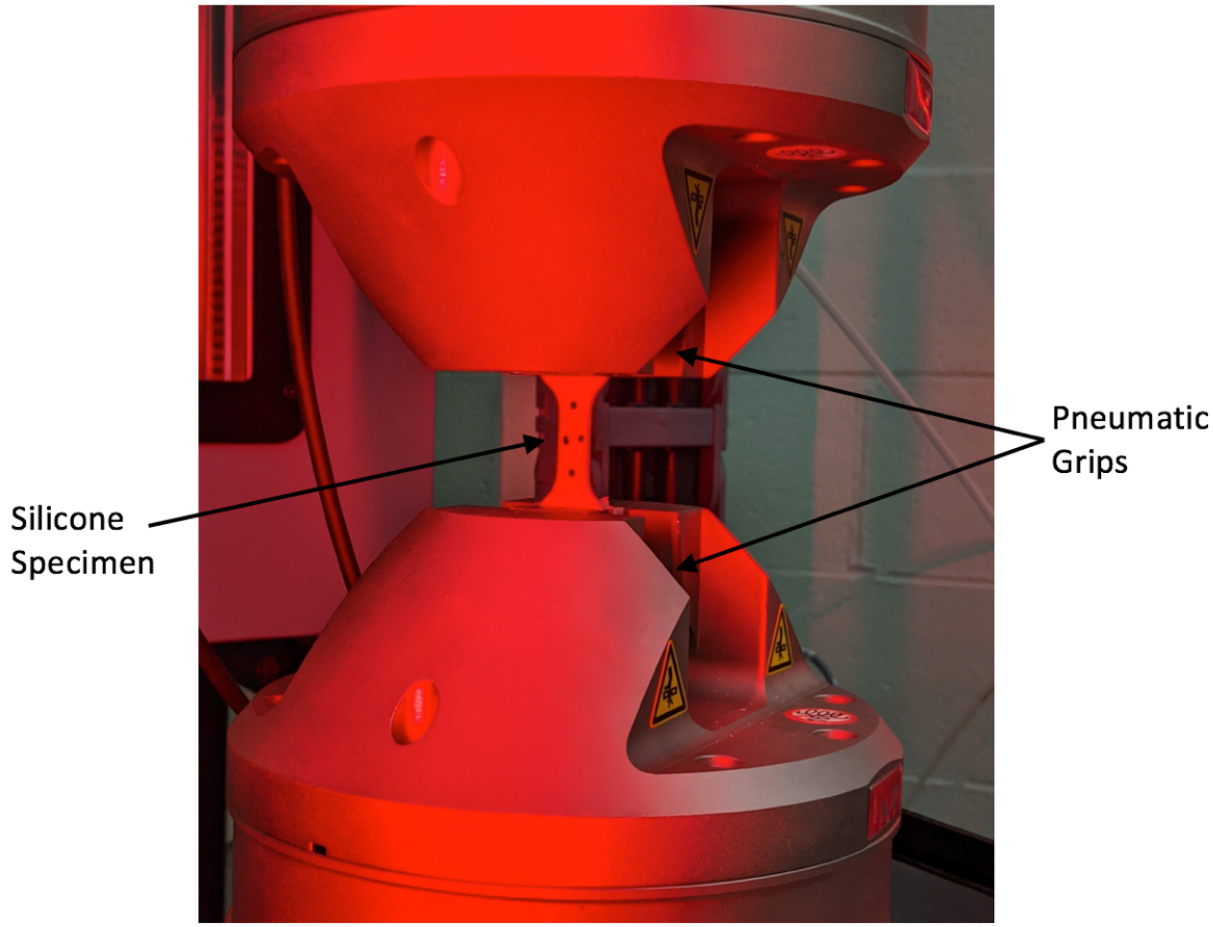


**Figure 3.4 Silicone specimen in INSTRON E10000**

All tests were completed with the specimen clamped at both ends by the pneumatic grips of the testing machine. Alignment was simplified by the fact that the end tabs of each specimen were specifically designed to match the surface area of the grips, allowing for consistent alignment. Once aligned and secured, the clamp separation was increase at small increments until the point at which there was no bend in the specimen, but the specimen was not taut.

## 3.2 Material Model

Engineering stress and engineering strain are approximations used to find the stress and strain based on the original dimensions of a specimen before it has been subjected to any loading. Engineering stress and engineering strain can be obtained with the follow equations [89]:

$$\sigma = \frac{F}{A} \tag{3.1}$$

$$\varepsilon = \frac{L - L_o}{L_0} = \frac{L}{L_o} - 1 \tag{3.2}$$

Where $\sigma$ is the engineering strain, $F$ is the applied force, $A$ is the cross-sectional area, $\varepsilon$ is the engineering strain, $L$ is the total length, and $L_o$ is the original length.

However, due to the nature of elastic materials, like silicone, these equations do not hold true as the cross-sectional area of the specimen changes as load is applied. As a result, to accurately analyze data from tensile tests using elastic materials, true stress and true strain must be found to allow for the instantaneous cross-sectional area. True stress and true strain can be obtained with the following equations

$$\sigma_T = \frac{F}{A_i} \tag{3.3}$$

$$\varepsilon_T = ln\,(1 + \varepsilon) \tag{3.4}$$

assuming the material is fully incompressible, then constant volume can be assumed

$$v_i = v_o \tag{3.5}$$

Where $v_o$ is the original volume, and $v_i$ is the instantaneous volume. Approximation allows,

$$A_i L_i = A_o L_0 \tag{3.6}$$

$$A_i = \frac{A_o(L_o)}{L_i} \tag{3.7}$$

By substituting equation 3-7 into equation 3-3, True Stress can be simplified to:

$$\sigma_T = \frac{F}{A_o}(1+\varepsilon) \tag{3.8}$$

Where $\sigma_T$ is the true stress, $F$ is the applied force, $A_i$ is the instantaneous cross-sectional area, $\varepsilon_T$ is true strain, and $\varepsilon$ is the engineering strain. Equations 3.4 and 3.8 were used to analyze the tensile test data collected and obtain stress-strain curves.

### 3.3 Hyperelastic Model

For this study the hyperelastic material properties of the silicone were evaluated, and based on previous literature, silicone was considered to be a "tissue-like" material for the aorta due to its compliance and hyperelastic behavior [39]–[48]. For hyperelastic computational studies of AAAs the most widely used strain energy function was originally proposed by Raghavan et al., which assumes the material is homogenous, incompressible and isotropic. [50] The following is the strain energy function proposed by Raghavan et al.

$$W = C_{10}(I_B - 3) + C_{20}(I_B - 3)^2 \tag{3.9}$$

where $W$ is the strain energy density, $I_B$ is the first invariant of the left Cauchy-Green tensor, and $C_{10}$, $C_{20}$ are the parameters for the material properties of their specimens. They then proposed a constitutive model for the case of a uniaxial tensile test,

$$T_1 = \left[2C_{10} + 4C_{20}\left({\lambda_1}^2 + 2{\lambda_1}^{-1} - 3\right)\right]\left[{\lambda_1}^2 - {\lambda_1}^{-1}\right] \tag{3.10}$$

where $T_1$ is traction, and $\lambda_1$ is stretch ratio. In the case of uniaxial tensile testing traction and stretch ratio can be found using the following equations,

$$T_1 = \frac{F}{A} \tag{3.11}$$

$$\lambda_1 = \frac{L}{L_o} \tag{3.12}$$

Equations 3.11 and 3.12 were used to analyze the tensile test data and plot $T_1 - \lambda_1$ data. To get the nonlinear best fit values of $C_{10}$ and $C_{20}$ for our data, our data was fit to equation 3.10 by using MATLAB R2018b to minimize the sum of square error.

### 3.4 Linearly Elastic Model

To determine the linear elastic material characteristics, elastic modulus and Poisson's ratio, the linear region of the stress-strain curve is analyzed. In this case the linear elastic region is only available at small strains. The elastic modulus is calculated by determining the slope of the stress-strain curve for only the linear region. The Poisson's ratio would ideally be calculated from the axial and transverse strains obtained from the Instron E10000 using equation 3.13 [89].

$$\nu = -\frac{\varepsilon_{Trans}}{\varepsilon_{Axial}} \tag{3.13}$$

Where $\nu$ is Poisson's ratio, $\varepsilon_{Trans}$ is transverse strain and $\varepsilon_{Axial}$is axial strain. Due to the nature of the silicone material, the black markers often stretched during the test making the measured axial and transverse strains not consistent. An alternative method to determine an equivalent Poisson's ratio can then be achieved from the following equations [89].

$$E = 2G(1 - \nu) \tag{3.14}$$

$$G = 2(C_{10}) \tag{3.15}$$

Substituting equation 3.14 into 3.15 and rearranging provides

$$\nu = \left(\frac{E}{2C_{10}}\right) - 1 \tag{3.16}$$

Where E is Elastic Modulus, G is shear modulus, and $C_{10}$ is the material constant.

## 3.5 Results and Discussion

The stress-strain response of each uniaxial test of the silicone specimens is shown in Figure 3.5. This result shows that there was minimal variation in the responses of each specimen, yielding consistent results from each test. It can also be observed that the behavior remained consistent when the thickness of the specimen was increased from 1.5mm to 3mm (Figure 3.6). The observed stress-strain behavior is also similar to that exhibited in the study completed by Raghavan et al. [79] when they performed uniaxial tensile testing on both aneurysmal and normal abdominal aortic tissue. Specifically, the stress-strain behavior exhibited by the silicone specimens in this study provided a stress-strain plot with a very similar shape to the plots produced by Raghavan et al. A comparison of "normal" aortic tissue from the study completed by Raghavan et al and the 1.5 mm silicone sample, can be seen in Figure 3.7. The data for the healthy aortic tissue was collected from the referenced paper using WebPlotDigitizer [90] and replotted such that the same units could be utilized.

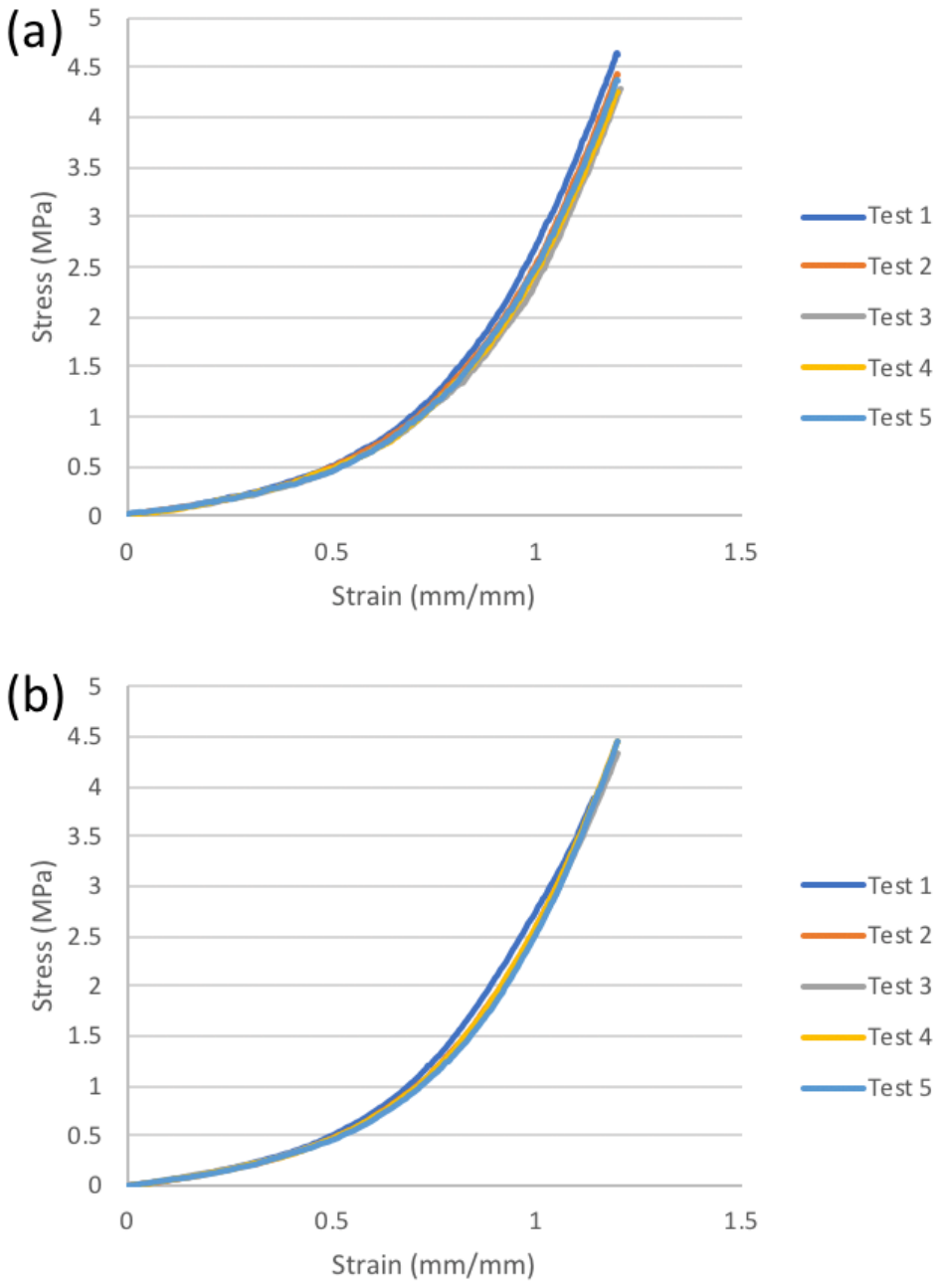


**Figure 3.5 Stress-strain curves for (a) 1.5mm and (b) 3mm Specimens**

10 silicone specimens were tested, five 1.5 mm specimens and five 3 mm specimens. Plotting the resulting stress-strain curves illustrated that there is minimal variation in the stress-strain response of each individual test.

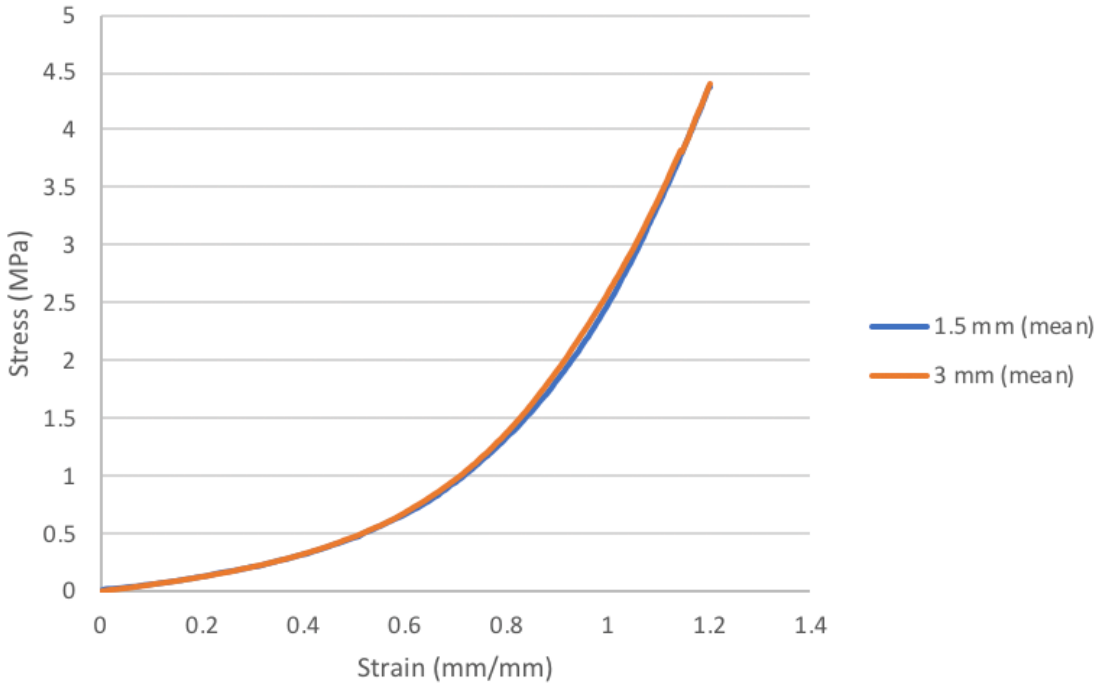


**Figure 3.6 Mean stress-strain curves for 1.5mm and 3mm specimen tests.**

Plotting the mean stress-strain curves for the 1.5 mm and 3mm specimen tests, from the tests plotted in figure 3.5, illustrates the consistency of the stress-strain response of the silicone material when there is a change in specimen thickness.

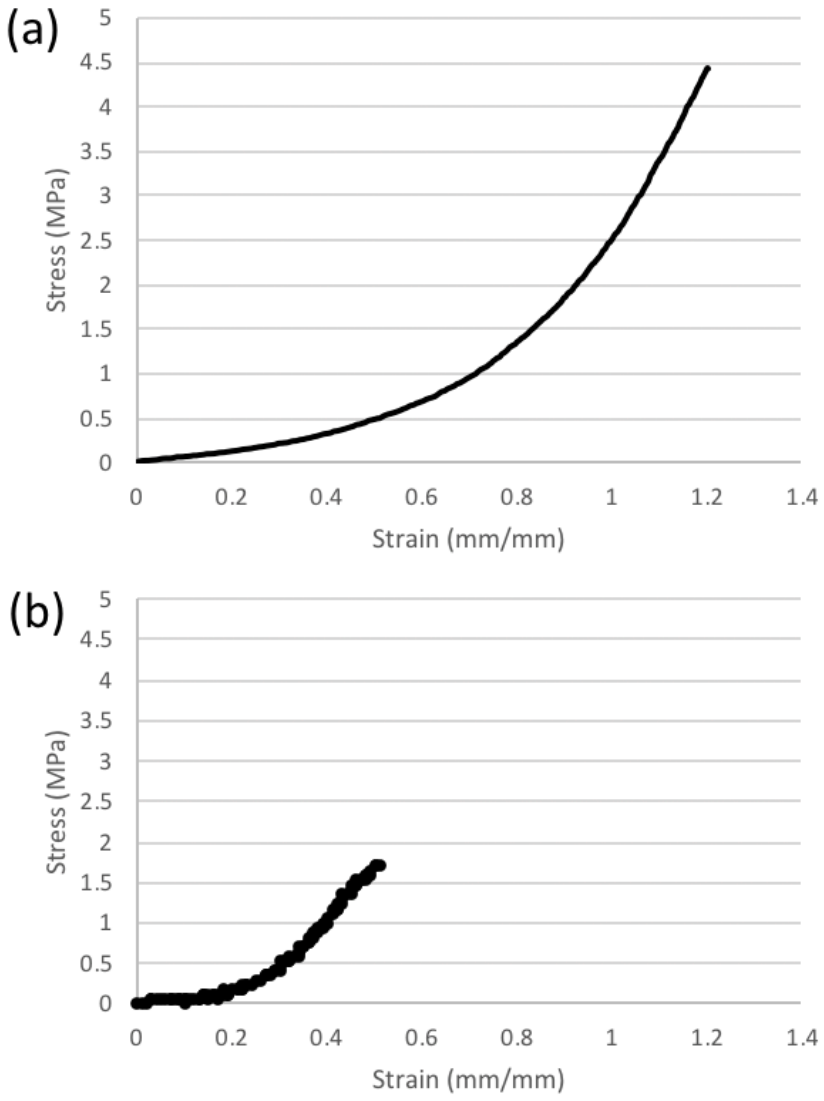


**Figure 3.7 Stress-strain curves (a) a 1.5 mm specimen and (b) a healthy human aortic tissue**

Each of the above plots show a single test specimen, one for a 1.5 mm silicone specimen and one of healthy aortic tissue tested by Raghavan et al. [79] The shape of the plots highlight that both materials exhibit similar stress-strain responses when subjected to uniaxial tensile testing.

The maximum true strain observed during each tensile test was approximately 1.19 mm/mm. When considering the silicone as a "tissue-like" material it had to be determined if additional testing would be required beyond the 1.19 mm/mm strain measured in our initial set of results. The average internal diameter of an aorta is recorded to be roughly 18.5 mm [87]. Current recommended practices for AAA intervention recommend medical intervention when the aneurysm reaches an internal diameter of 55 mm. [21] These diameters can be correlated to strains using the following equation to find engineering strain,

$$\varepsilon = \frac{C - C_0}{C_0} \tag{3.13}$$

Where $C_0$ is the original circumference, and $C$ is the expanded circumference. This engineering strain can then be used in Equation 3.4 to find the true strain associated with the expanded diameter. These results can be seen in table 3.1.

However, it has been reported [91] that 10-15% of all aneurysm rupture prior to reaching the 55mm diameter. As a result, the critical strain values to consider for computational studies of AAAs should be those up to 1.0895 mm/mm (or approximately 1.1 mm/mm). Considering the strain associated with a diameter of 5.5 cm to be the critical strain will allow for conservative estimates when performing computational studies. This means the maximum strain of approximately 1.19 mm/mm observed in the tensile testing for this study is sufficient as it exceeds the critical strain of 1.1 mm/mm.

For each set of data that was collected and analyzed during this study the best non-linear fit hyperelastic constants were determined (Table 3.2) by minimizing the sum of square error in MATLAB R2018b.

The mean values of these constants were then calculated (Table 3.3). The mean values are the constants that were subsequently used for computational analysis. The percent different between the 1.5 mm and 3 mm thick silicone specimens was calculated using equation 3.14.

$$Percent\ error = \left|\frac{1.5\text{ mm Constant} - 3\text{ mm Constant}}{3\text{ mm Constant}}\right| x100\% \qquad (3.14)$$

With a percent error of 2.29 and 3.53 for $C_{10}$ and $C_{20}$ respectively for their mean values, it can be noted there is minimal effect on the outcome of the hyperelastic constants based on the thickness of the specimen for this material.

The elastic modulus from the average values of the elastic moduli for each test, and the corresponding Poisson's ratio was calculated using the $C_{10}$ calculated from the hyperelastic non-linear fit. The resulting elastic modulus and Poisson's ratio can be found in Table 3.4. For silicone materials the expected Poisson's ratio is typically within the range of 0.48-0.5 [92]. The calculated Poisson's ratio of 0.4844 falls within the expected range providing confidence in the calculated result.

**Table 3.1 Values used to determine strain associated with recommended aneurysm intervention diameter of 55 mm**

| Average Aorta Diameter (mm) | Circumference (mm) | Intervention Diameter (mm) | Intervention Circumference (mm) | True Strain (mm/mm) |
|---|---|---|---|---|
| 18.5 | 58.1194 | 55 | 172.7875 | 1.0895 |

**Table 3.2 Best fit hyperelastic constants for uniaxial tensile tests of 1.5 mm and 3 mm specimens**

| Specimen # | Thickness = 1.5 mm | | Thickness = 3 mm | |
|---|---|---|---|---|
| | $C_{10}$ (MPa) | $C_{20}$ (MPa) | $C_{10}$ (MPa) | $C_{20}$ (MPa) |
| 1 | 0.1275 | 0.0057 | 0.1281 | 0.0064 |
| 2 | 0.1201 | 0.0055 | 0.1204 | 0.0057 |
| 3 | 0.1151 | 0.0053 | 0.1232 | 0.005 |
| 4 | 0.1164 | 0.0052 | 0.123 | 0.0054 |
| 5 | 0.1159 | 0.0056 | 0.1147 | 0.0058 |

**Table 3.3 Mean values of hyperelastic material constants for both 1.5mm and 3mm specimens. SD represents the standard deviation.**

| Thickness = 1.5 mm | | | | Thickness = 3 mm | | | |
|---|---|---|---|---|---|---|---|
| $C_{10}$ (MPa) | SD | $C_{20}$ (MPa) | SD | $C_{10}$ (MPa) | SD | $C_{20}$ (MPa) | SD |
| 0.119 | 0.004618 | 0.00546 | 0.0001854 | 0.12188 | 0.004368 | 0.00566 | 0.0004630 |

**Table 3.4 Linearly Elastic Material Properties. SD represents the standard deviation**

| Average Elastic Modulus (MPa) | SD | Poisson's Ratio |
|---|---|---|
| 0.7131 | 0.0272 | 0.4844 |

## 3.6 Limitations

As noted in section 3.4, ideally the Poisson's ratio would be established using an extensometer. The video extensometer that the INSTRON E10000 is equipped with had challenges when it was used with a silicone material as the deformation due to stretch of the silicone made it difficult to maintain consistent fiducial markers. Alternatively, a numerical approach was utilized to determine a Poisson's ratio. The determined Poisson's ratio falls within the expected range of Poisson's ratios for silicone materials. As a result, it is not expected that using the numerical approach to determine the Poisson's ratio significantly impacts the resulting value in this study. However, if further testing or retesting of this material were to be completed for the Poisson's ratio, it would be recommended to use an extensometer that is more compatible with an extensible material, such as a video extensometer that does not require markers, or a contacting extensometer. Additionally, to determine the hyperelastic coefficients that would be suitable for a larger range of deformation, testing would have to be completed on a machine that can allow for a larger stroke during testing.

## 3.7 Conclusions

In this chapter the hyperelastic constants, correlating with the strain energy function proposed by Ragahavan et al [50], were determined using Smooth-Sil 940 as a "tissue like" material. This material was tested and analyzed for specimens of two different thicknesses, 1.5 mm and 3 mm. The results of the stress-strain analysis for the material was consistent for both the 1.5 mm specimens and the 3 mm specimens, and aligned with the stress-strain behavior exhibited by abdominal aortic tissue in the study completed by Raghavan et al. [79]. This finding provided partial validation that, with respect to the stress-strain behavior, silicone can be treated as a "tissue like" material when comparing it with aortic tissue. In addition to this finding, from the

hyperelastic constants that were determined for specimens of both thicknesses, we were able to conclude that the thickness of the specimen has minimal effect on the outcome of the hyperelastic properties of the material. The resulting linear elastic material properties were also calculated for future use.

# Chapter 4 Investigating an Area of Reduced Wall Thickness as a Mechanism for Abdominal Aortic Aneurysm Initiation Using Commonly Used Computational Material Models and "Tissue-like" Material.

Understanding initiation of AAAs could allow for the generation of more diagnostic and preventative care options for those at high risk for the development of AAAs. Due to the complexity associated with using human tissue for research, many studies on this topic are completed computationally. Computational studies have often made assumptions that simplify the complex nature of the aorta's geometry and material behavior. Many of the studies that had been reviewed assumed linearly elastic or hyperelasric properties. In the case of a hyperelastic model, most often a reduced polynomial strain energy function (SEF) (see Eq. 4.1) was utilized and the constants were assumed to be those proposed by Raghavan et al. [50]

$$W = C_{10}(I_B - 3) + C_{20}(I_B - 3)^2 \tag{4.1}$$

where $W$ is the strain energy density, $I_B$ is the first invariant of the left Cauchy-Green tensor, and $C_{10}$, $C_{20}$ are the parameters for the material properties of their specimens. Though this SEF and proposed constants were often utilized, to the best of the authors knowledge, no additional testing had been completed to validate the resulting computation model as a valid approximation to experimental results.

To date the only known computational investigation completed that considered the initiation of abdominal aortic aneurysms was the study completed by Simsek and Kwon [38]. In their study they considered regions of their simplified model to "degeneration zone", having reduced elastic modulus and material constants. In this chapter, the result of implementing an area

of reduced wall thickness is investigated computationally and experimentally. The experimental tests used the silicone investigated in chapter 3 to create simplified models, the material properties of this silicone were used in the simplified computational models so their results could be compared.

## 4.1 Computational Studies - Finite Element Analysis

Four computational studies were completed to compare with experimental results. Each of these studies was completed using the software ABAQUS (v6.14).

### 4.1.1 Model Geometry

Two geometrical models were generated with a simplified geometry to mimic the dimensions of an abdominal aorta. One model maintains a uniform wall thickness with no defects, while the other model has an area of reduced wall thickness that constitutes the aneurysm region. The details of the geometry for these models can be found in Figure 4.1. The diameters and wall thickness selected for the uniform wall thickness model were based on the recorded abdominal aortic aneurysm listed in the handbook of biomaterial properties[87]. The reduced wall thickness model uses the same vessel geometry with the exception of a 12mm region at the middle of the model where the thickness is reduced from 1mm to 0.625 mm. The reduced thickness model was utilized to investigate if the reduction of the wall thickness causes an aneurysmal shape to form when subjected to internal pressures.

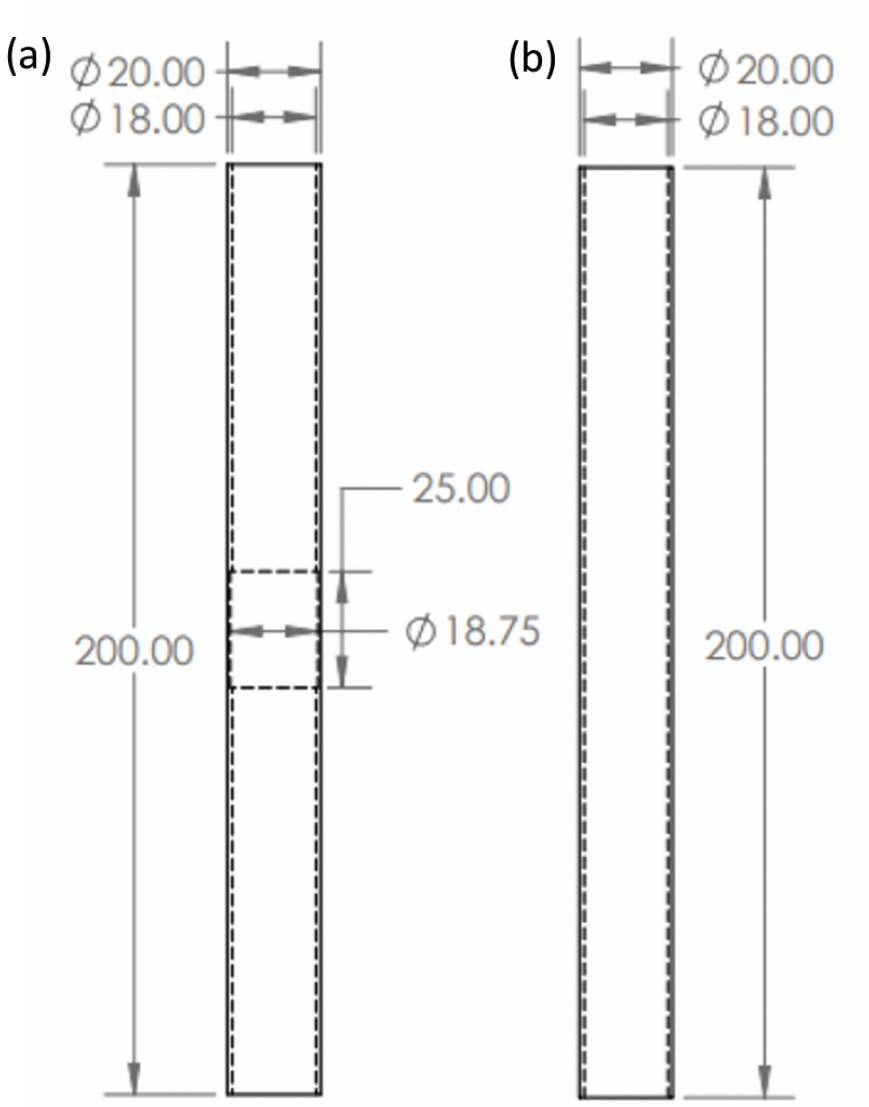


**Figure 4.1 Geometry for computational and experimental models.**

Two geometrical models (a) Reduced wall thickness model and (b) Uniform wall thickness model were created and used for both the computational and experimental models for this study (all indicated dimensions are in mm).

### 4.1.2 Material Models

Four computational models were constructed using ABAQUS (v 6.14). These models were built using the model geometry described in section 4.1.1, and applying linearly elastic and hyperelastic material models to each geometrical model. The hyperelastic material model used for these investigations was a reduced polynomial, (Eq. 4.1) as this is the most commonly used hyperelastic material model utilized when investigating abdominal aortic aneurysms. In chapter three the uniaxial tensile testing of silicone and the process of obtaining the corresponding material properties from the data was detailed. The resulting linearly elastic properties and hyperelastic constants can be found in table 4.1.

**Table 4.1 Material properties for Smooth-Sil 940 obtained from uniaxial tensile testing. Details of tensile testing are in Chapter 3**

| Linearly Elastic Properties | | Hyperelastic Constants | |
|---|---|---|---|
| Elastic Modulus (MPa) | Poisson's Ratio | $C_{10}$ (MPa) | $C_{20}$ (MPa) |
| 0.7131 | 0.4844 | 0.12188 | 0.00566 |

### 4.1.3 Mesh Convergence

Each of the linearly elastic models were meshed with S8R elements. These elements contain more nodes per element, and as a result allow for more degrees of freedom and quicker convergence. The hyperelastic models were meshed with S4R elements. Maintaining the S8R elements with higher degrees of freedom for fewer elements would be ideal, however S8R elements are not compatible with hyperelastic materials. Mesh convergence studies were completed for each of the four computational models. These studies were completed by running each simulation with progressively finer meshes. The deformation was recorded at the same geometric location for each run, which can be seen in Figure 4.2. The results from these studies can be found in figure 4.3. From the completed studies it was deemed the linearly elastic models required a less refined mesh to converge to an acceptable solution, whereas the hyperelastic models required a more refined mesh. An "acceptable solution" was deemed to be achieved when the next mesh refinement resulted in a change in the max principal stress being less than 5%. At the chosen mesh refinement, the percent change between the last refinements were 0.03, 3.94, 0.05, and 0.965 for constant wall thickness elastic model, constant wall thickness hyperelastic model, area of reduced wall thickness elastic model, and area of reduced wall thickness hyperelastic model respectively.

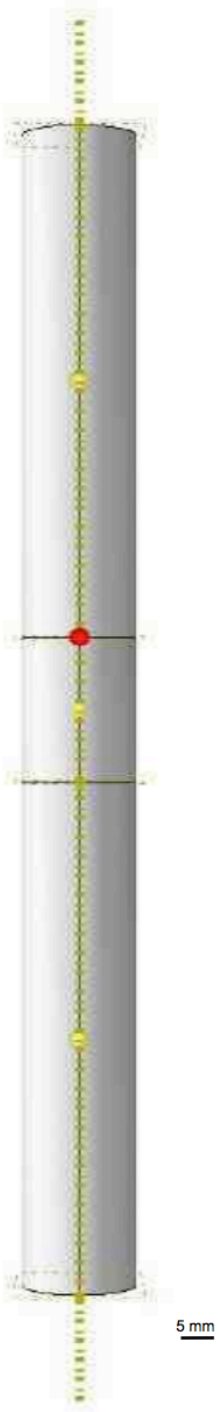


**Figure 4.2 Measurement location for mesh convergence studies.**

The red dot in the figure highlights the location where the deformation was recorded for each mesh refinement of the mesh convergence study.

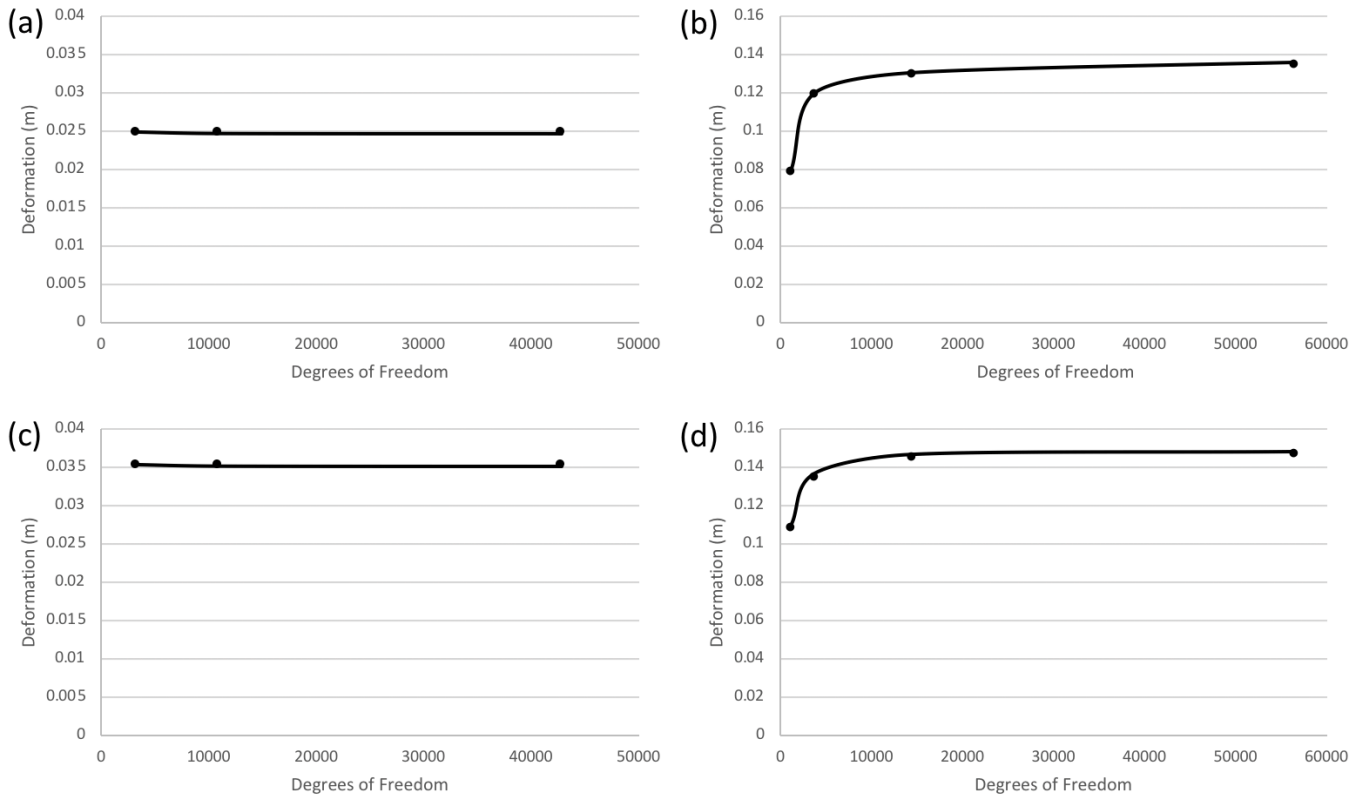


**Figure 4.3 Mesh convergence studies completed for each computational model**

Four mesh convergence studies were completed, one for each computational model (a) Linearly Elastic Uniform Wall Thickness Model (b) Hyperelastic Uniform Wall Thickness Model (c) Linearly Elastic Reduced Wall Thickness Model (d) Hyperelastic Reduced Wall Thickness Model. The plotted results show how the mesh converges as the mesh is refined

### 4.1.4 Computational Pressure Testing

Each computational model was subjected to internal pressures correlating with 60 to 210 mmHg. These pressures were chosen to encompass the range of pressures typically experienced in vivo. In addition, each model was subjected to a force of 0.235 N at the bottom of the model to reflect the force due to the weight of the pressure transducer, spacer, and associated fittings (Fig 4.4) that were present during experimental data collection. Boundary conditions were applied to each end of the model. The boundary condition at the top of the model was fully fixed (U1=U2=U3=UR1=UR2=UR3=0) while the bottom boundary condition allows for movement in the Y-direction (no specified value for U2). The change in diameter at the middle of the model was extracted for each test. In the event that there is not a single node at the middle of the model, the average value between the two nodes nearest to the middle was taken.

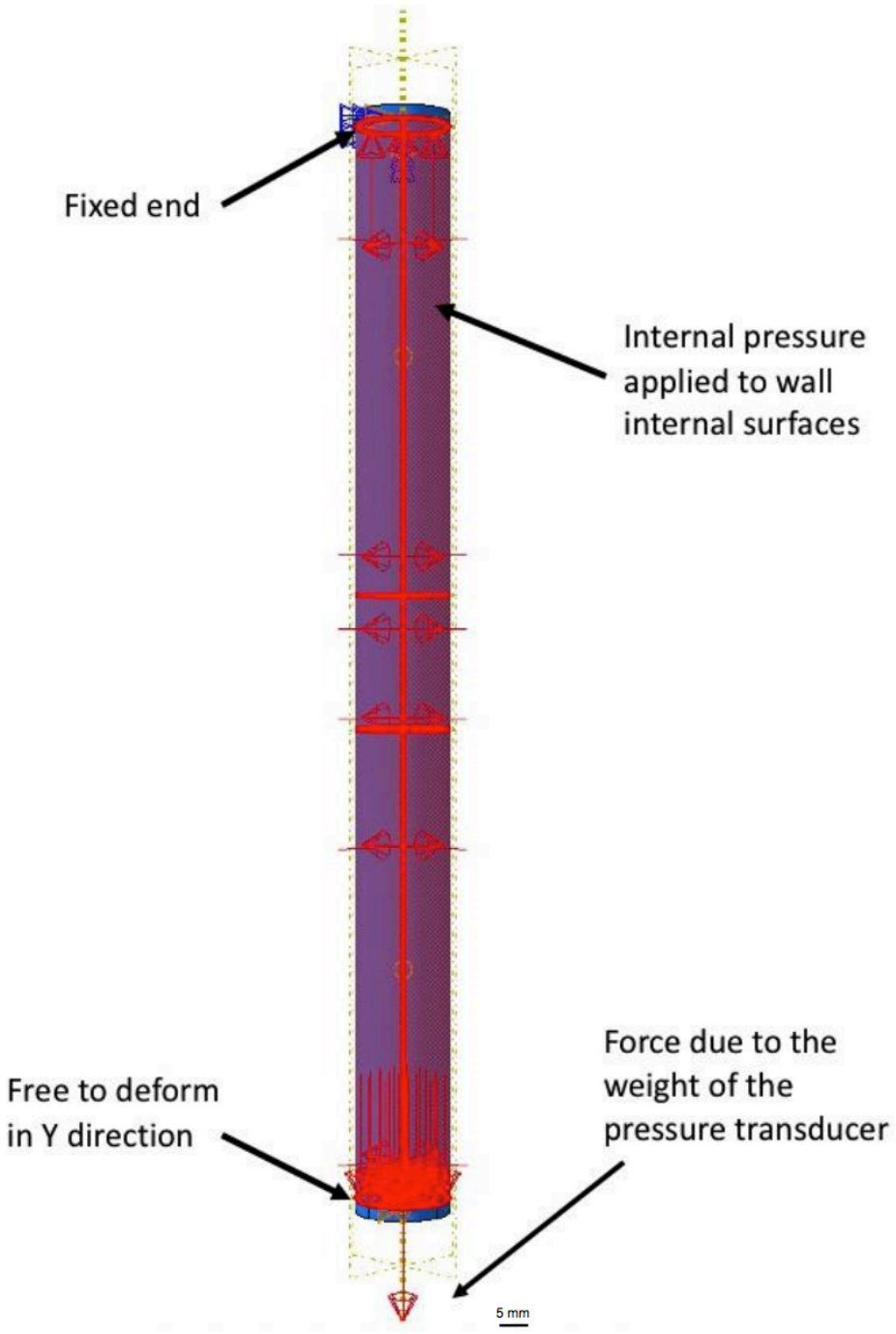


**Figure 4.4 Applied boundary conditions and internal loading.**

The top boundary condition is restrained in all directions, the bottom boundary condition allows translation along the Y axis. Internal pressure is applied to the inside of the and on both the top and bottom ends. An additional downward force of 0.235 N was applied to the bottom of the bottom to account for the weight of the transducer, spacer and fittings used in the experiments.

## 4.2 Experimental Testing

An experimental test set-up was built to directly compare the physical silicone model with computational models; the test set-up was designed to record the change in radius of the test specimens while being subjected to internal pressures.

### 4.2.1 Specimen Fabrication

The specimens for the experimental testing were fabricated using Smooth-Sil 940 (Smooth-On, Macungie). This silicone material was utilized because the properties applied to the computational models were those determined from testing this "tissue-like" silicone material in Chapter 3. To achieve geometry as similar as possible to those used in the computational models, a precise specimen mold was required.

All molds were fabricated in consultation with the Technical Services department at Memorial University. The initial mold design is shown in Figure 4.5. The mold was printed on a 3D printer. However, the resulting tubes were not smooth or consistent, and often resulted in ridges and breakage. As a result, a refined mold was designed and fabricated (Fig 4.6). This mold was machined from aluminum to ensure a smooth inner surface. The resulting tubes from this mold were free of seams, smooth and consistent, Figure 4.7 shows the difference between the resulting tubes from each mold.

Using the aluminum mold, six specimens were fabricated. Three specimens were fabricated with a uniform wall thickness, and three were fabricated with an area of reduced wall thickness to

reflect the geometry from Figure 4.1. The area of reduced wall thickness was achieved by using a metallic tape on the internal shaft to increase the internal diameter at the middle of the silicone tube. For each specimen, the silicone was mixed as per the manufacturer instructions, including time under a vacuum to ensure there are no trapped air bubbles. The silicone was then poured into the tube mold until the mold was completely filled. Once the mold was filled, the silicone was left to cure for a minimum of 24 hours prior to being removed from the mold.

To verify that the thickness of the silicone tube specimens was remaining consistent along the length of the model, test tubes were cut longitudinally and the wall thickness was measured using a FARO platinum arm with a V3 laser scanner. The results of the laser scan measurements can be found in Table 4.2. There is a small standard deviation, however the laser scanner itself has a tolerance of +/- 0.064 mm. [93] All measurements were within the listed tolerance.

**Table 4.4.2 Average values and standard deviations (SD) of tube specimen wall thickness from laser scan**

| Standard Wall Thickness (mm) | SD | Area of Reduced Wall Thickness (mm) | SD |
|---|---|---|---|
| 0.985 | 0.0437 | 0.625 | 0.0108 |

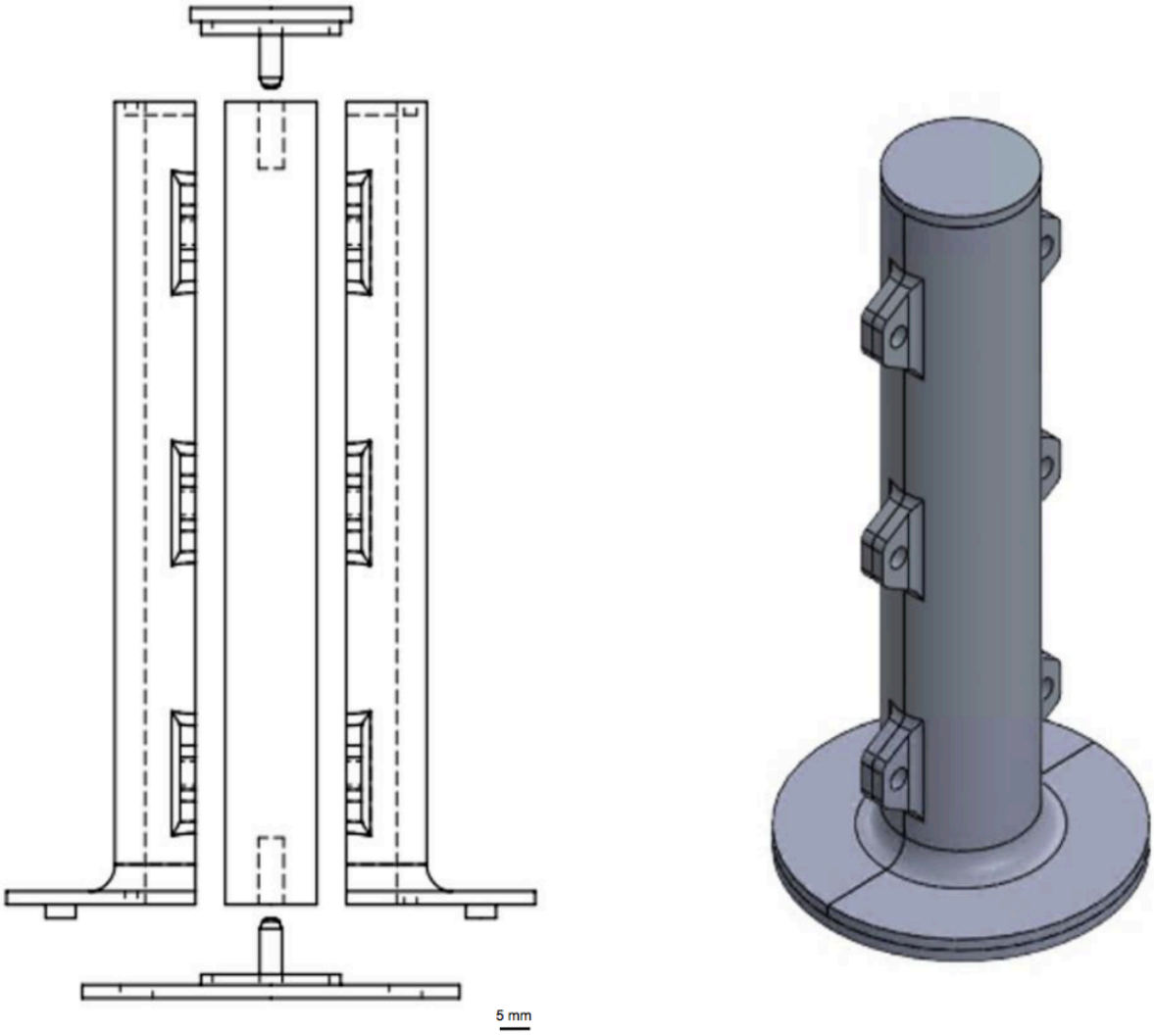


**Figure 4.5 Initial mold design for silicone tube specimens.**

The initial mold design was designed to be 3D printed. However, the resulting texture from the 3D printed material was not adequately smooth, in addition the design of the mold having two halves often resulted in ridges at the seams of the tube specimens and breakage near the seams upon removal from the mold. The left hand side of the figure shows an exploded side view of the model. The dashed lines show the internal diameter of the part and holes were end cap pins insert. The right hand side of the figure shows an isometric view the mold fully assembled.

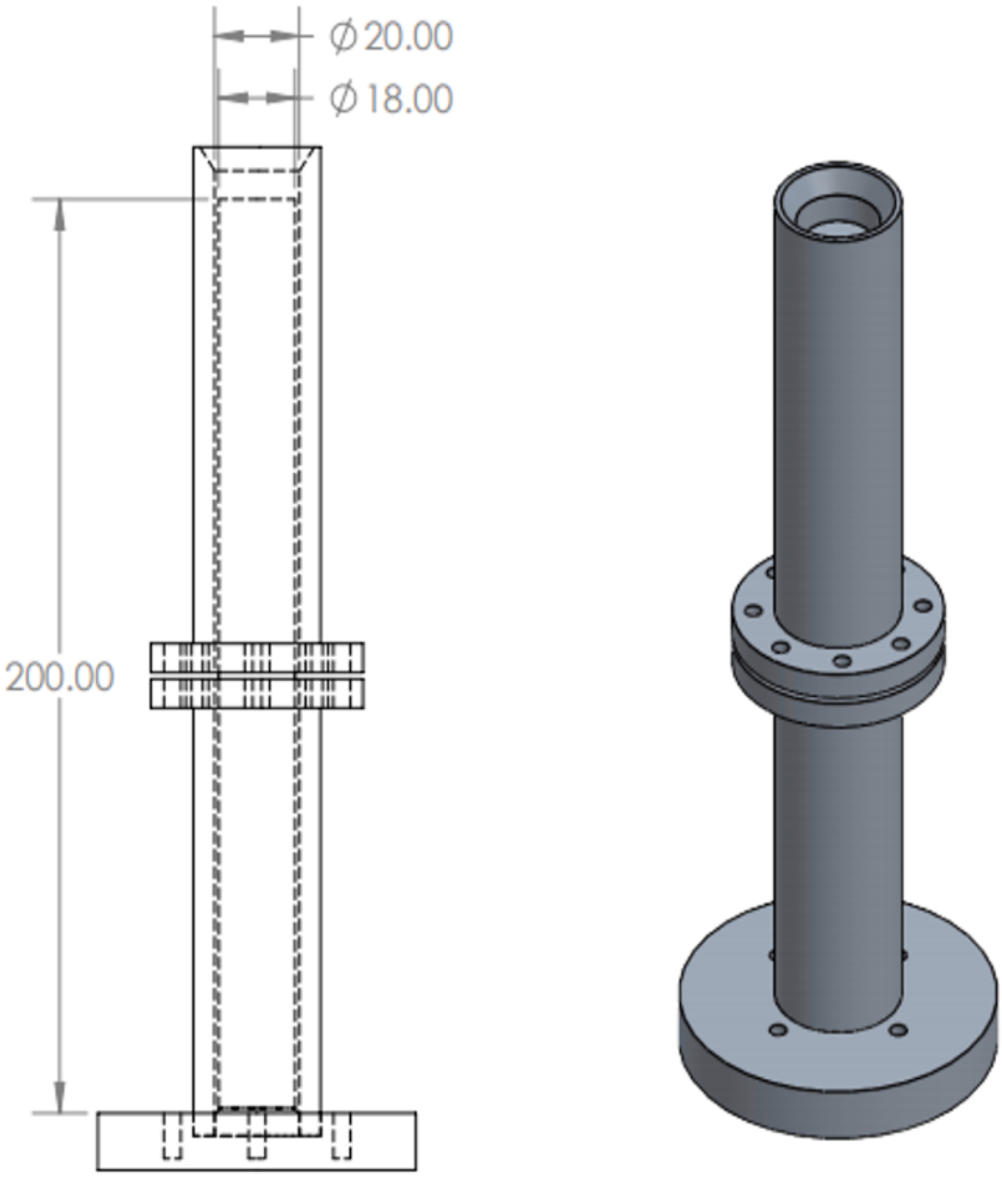


**Figure 4.6 Final mold design for silicone tube specimens.**

The final mold design was designed to be machined out of aluminum. The resulting tubes were smooth and consistent. There were no visible seems where the mold halves connected and no breakage experienced upon removal from the mold. The left hand side of the figure shows a side view of the final mold assembled, the dashed lined show the inside diameters and the internal shaft as well as the holes where the mold is bolted to ensure alignment (indicated dimensions are provided in mm).

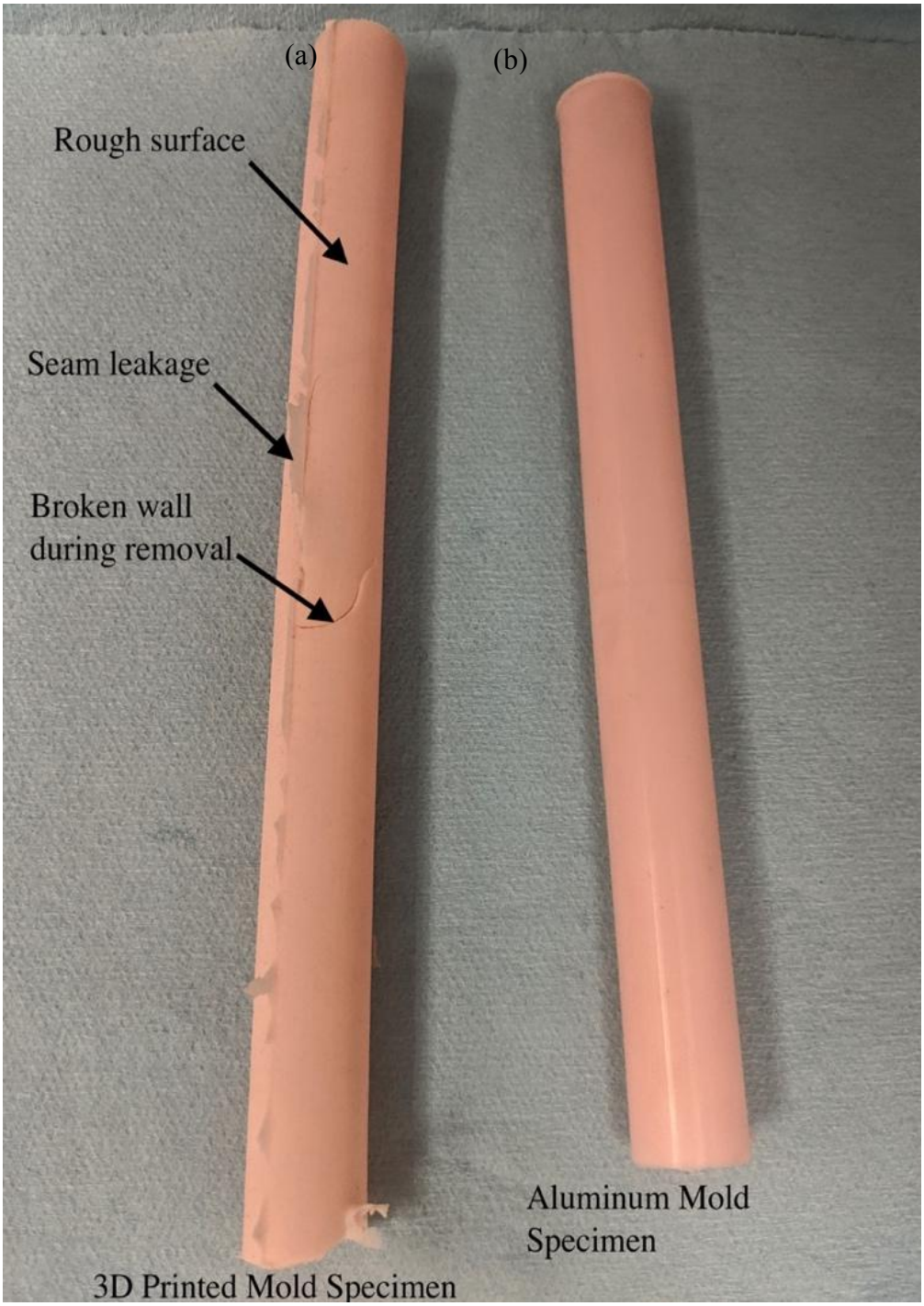


**Figure 4.7 Resulting tube specimen from (a) 3D printed mold (b) aluminum mold**

The silicone tubes resulting from the aluminum mold were significantly smoother than those produced with the 3D printed mold. The 3D printed tube specimens experienced a number of issues highlighted in the figure such as a rough surface, seams and breakage.

### 4.2.2 Experimental Test Set-up

For pressure testing a small biological vessel it is common to use a pressure myograph system. A pressure myograph often consists of a vessel being mounted horizontally in a pressure myograph chamber, and subjected to internal pressure. Video with an inverted microscope is used to capture the continuous diametrical changes. [94]–[96] Recreating the set-up of a commercial pressure myograph system was not feasible for the size of specimen being used, in combination with the equipment readily available. Using concepts of the pressure myograph system as a guide, combined with the resources available on site, a test set-up was designed to pressure test the silicone specimens.

To avoid any sagging at the mid region of the specimens due to gravity the specimens were mounted vertically on a retort stand secured with a burette clamp (Fig. 4.9). Each end of the specimens were mounted onto plastic spacers, the plastic spacers were machined to achieve a press fit with the 1/8" tubes (Fig. 4.8). At the top of the test set-up the 1/8" tube feeds the pressure inducing medium, for these tests the medium was air. The air was pumped into the specimens using a Harvard Apparatus PHD 2000 syringe pump with a 60 ml syringe. At the bottom end of the specimen the small 1/8" tube attaches to a pressure transducer for a Digi-Med Blood Pressure Analyzer (BPA) (Digi-Med, Kentucky, USA) to continuously monitor the applied internal pressure. The Digi-Med PBA has a range of -50 to 350 mmHg and a tolerance of +/- 0.2 mmHg. A schematic of this set-up can be seen in Figure 4.9 A sheet of black grid paper with a separation of 5 mm between each grid line was mounted behind the specimen. The black grid paper acts as a scale for reference to ensure an accurate measurement of the change in diameter, while also providing adequate contrast with the silicone specimens. A Nikon 5600 DSLR camera with a 24.2-

megapixel resolution was arranged to ensure the video is in the same plane with the silicone specimens. This required making small adjustments to the silicone specimens to ensure they were as aligned as possible in all views. The full test set-up can be seen in Figure 4.9.

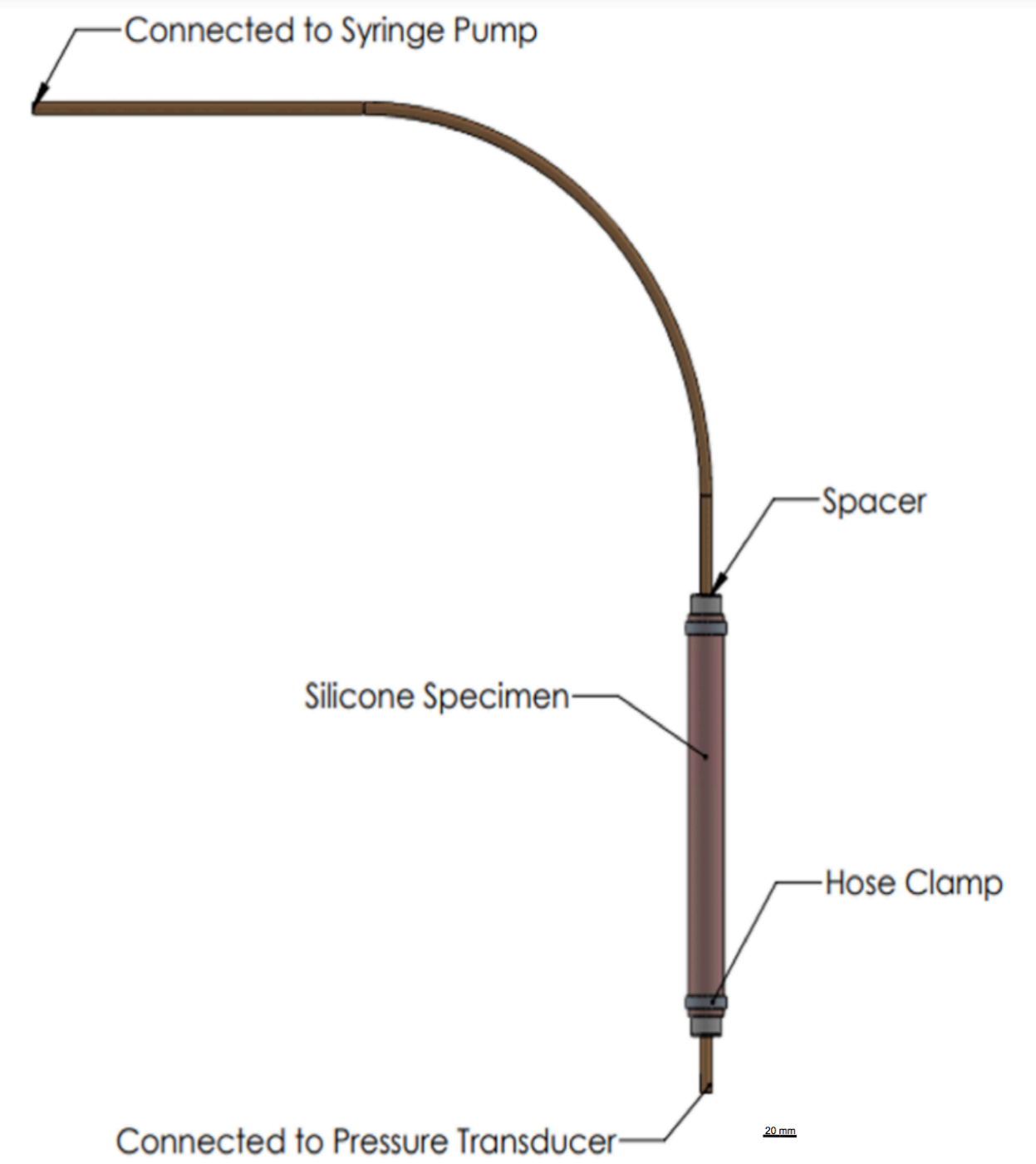


**Figure 4.8 Set-up of tube specimens during experimental testing.**

The silicone tube specimens were mounted on machined plastic spacers and secured with hose clamps. 1/8" tubing is press fit into the plastic spacers and run to the syringe pump and pressure transducer.

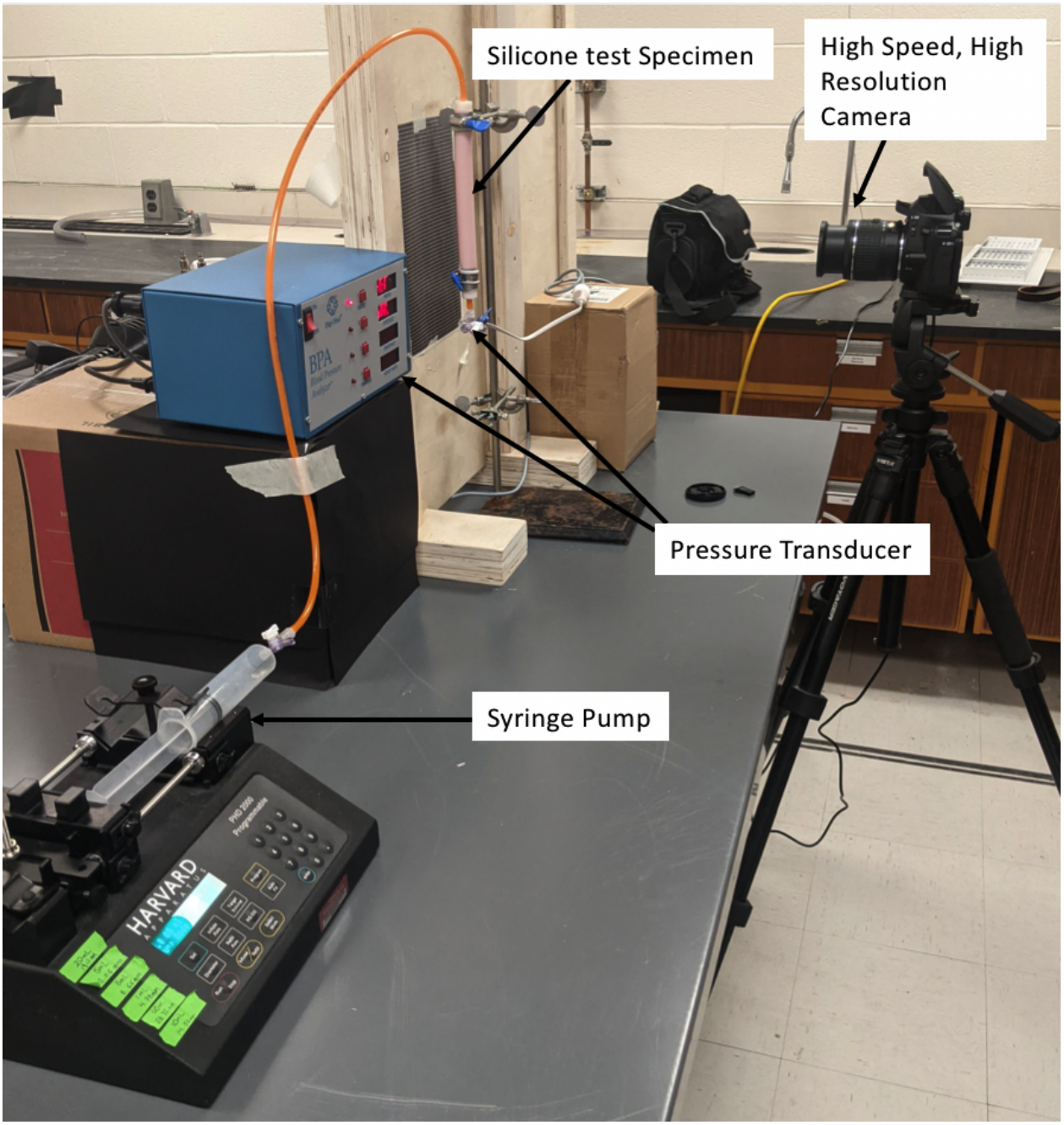


**Figure 4.9 Experimental test set-up for pressure testing silicone tube specimens**

The test set-up consists of a high speed camera positioned to be in plane with the silicone test specimens. The black grid paper behind the specimen allows for adequate contrast and accurate deformation measurements. The top of the tube specimen is connected to a syringe pump that subjects the tube specimen to internal pressure. The bottom of the specimen is connected to a pressure transducer so the real-time pressure experienced by the tube can be recorded.

### 4.2.3 Experimental Pressure Testing

The experimental pressure tests were completed by completing the following steps:

1. Calibrate the Digi-Med Blood Pressure Analyzer (BPA) using a sphygmomanometer to verify the BPA is accurately measuring the applied pressure as per manufacturer's instructions. BPA was zeroed to atmospheric pressure and calibrated at 100 mmHg.
2. Ensure all valves are closed to the environment.
3. Verify alignment of silicone specimen.
4. Turn on video camera
5. Turn on syringe pump to apply load.
6. When additional air is required, stop the pump, and close the valve at the start of the system nearest to the syringe is closed so pressure is maintained.
7. Refill syringe and reinstall into pump.
8. Open valve nearest to the pump and turn pump back on.
9. Repeat steps 6-8 if required. (this was typically completed 1-2 times to reach the maximum pressure of 210 mmHg)
10. Turn off the pump when the desired pressure has been reached
11. Turn off camera.

The videos correlating to each test were then uploaded onto a computer. On the computer the frames corresponding to each required pressure are extracted from each test. Each frame was then analyzed using an image processing software. The software MIPAR version 3.4.1 was utilized to manually measure the deformation of the specimens using the grid background to calibrate the measurements. When the deformations (which are assumed to be isotropic) are recorded for each test, the average result is taken for the uniform wall thickness models and reduced wall thickness

models. This allows for the deformation from the experimental models to be compared to the deformation of the computational models at each pressure.

## 4.3 Results and Discussion

The deformation was obtained for each model as described in sections 4.1.4 and 4.2.3 and recorded into table 4.3. Plotting these results (Fig 4.10) showed that for pressures within the range of excepted blood pressures in a human (up to 140 mmHg) the hyperelastic model did follow a similar trend to the experimental results.

**Table 4.3 Results of experimental and computational pressure testing. SD represents the standard deviation for the experimental tests.**

| Pressure (mmHg) | Data Source | Uniform Wall Thickness Change in Radius (mm) | SD | Reduced Wall Thickness Tube (Reduced Area) Change in Radius (mm) | SD |
|---|---|---|---|---|---|
| 0 | Computational (Elastic) | 0 | - | 0 | - |
| | Computation (Hyperelastic) | 0 | - | 0 | - |
| | Experiment (Average) | 0 | 9.428E-05 | 0 | 9.428E-05 |
| 20 | Computational (Elastic) | 0.002062 | - | 0.003284 | - |
| | Computational (Hyperleastic) | 0.000208 | - | 0.0003015 | - |
| | Experiment (Average) | 0.0002833 | 0.0001414 | 0.0007 | 0.0003771 |
| 40 | Computational (Elastic) | 0.004377 | - | 0.0069719 | - |
| | Computation (Hyperelastic) | 0.0004655 | - | 0.000769 | - |
| | Experiment (Average) | 0.0007166 | 0.0003091 | 0.001483 | 0.0006128 |
| 60 | Computational (Elastic) | 0.006693 | - | 0.010655 | - |
| | Computational (Hyperleastic) | 0.0007636 | - | 0.001361 | - |
| | Experiment (Average) | 0.001066 | 0.0003681 | 0.002516 | 0.0007257 |

| | | | | | |
|---|---|---|---|---|---|
| 80 | Computational (Elastic) | 0.009008 | - | 0.01434 | - |
| | Computation (Hyperelastic) | 0.001127 | - | 0.002159 | - |
| | Experiment (Average) | 0.001766 | 0.0002624 | 0.0043 | 0.002574 |
| 100 | Computational (Elastic) | 0.01132 | - | 0.01803 | - |
| | Computational (Hyperleastic) | 0.001533 | - | 0.003383 | - |
| | Experiment (Average) | 0.002433 | 0.0003559 | 0.009116 | 0.009027 |
| 120 | Computational (Elastic) | 0.01363 | - | 0.02172 | - |
| | Computation (Hyperelastic) | 0.002069 | - | 0.006083 | - |
| | Experiment (Average) | 0.003266 | 0.0006944 | 0.01203 | 0.008764 |
| 140 | Computational (Elastic) | 0.01595 | - | 0.02540 | - |
| | Computational (Hyperleastic) | 0.002806 | - | 0.01627 | - |
| | Experiment (Average) | 0.004683 | 0.0007257 | 0.0144 | 0.0062914 |
| 160 | Computational (Elastic) | 0.01827 | - | 0.029095 | - |
| | Computation (Hyperelastic) | 0.004065 | - | 0.0244555 | - |
| | Experiment (Average) | 0.00593 | 0.000828654 | 0.01581 | 0.0058804 |
| 180 | Computational (Elastic) | 0.02057 | - | 0.03277 | - |

| | | | | | |
|---|---|---|---|---|---|
| | Computational (Hyperleastic) | 0.01052 | - | 0.03032 | - |
| | Experiment (Average) | 0.007016 | 0.000828654 | 0.03277 | 0.006205 |
| 200 | Computational (Elastic) | 0.0229 | - | 0.03647 | - |
| | Computation (Hyperelastic) | 0.0258 | - | 0.03498 | - |
| | Experiment (Average) | 0.008016 | 0.001347 | 0.017383 | 0.006328 |
| 210 | Computational (Elastic) | 0.02405 | - | 0.03831 | - |
| | Computational (Hyperleastic) | 0.0258 | - | 0.03655 | - |
| | Experiment (Average) | 0.008016 | 0.001291 | 0.01811 | 0.006902 |

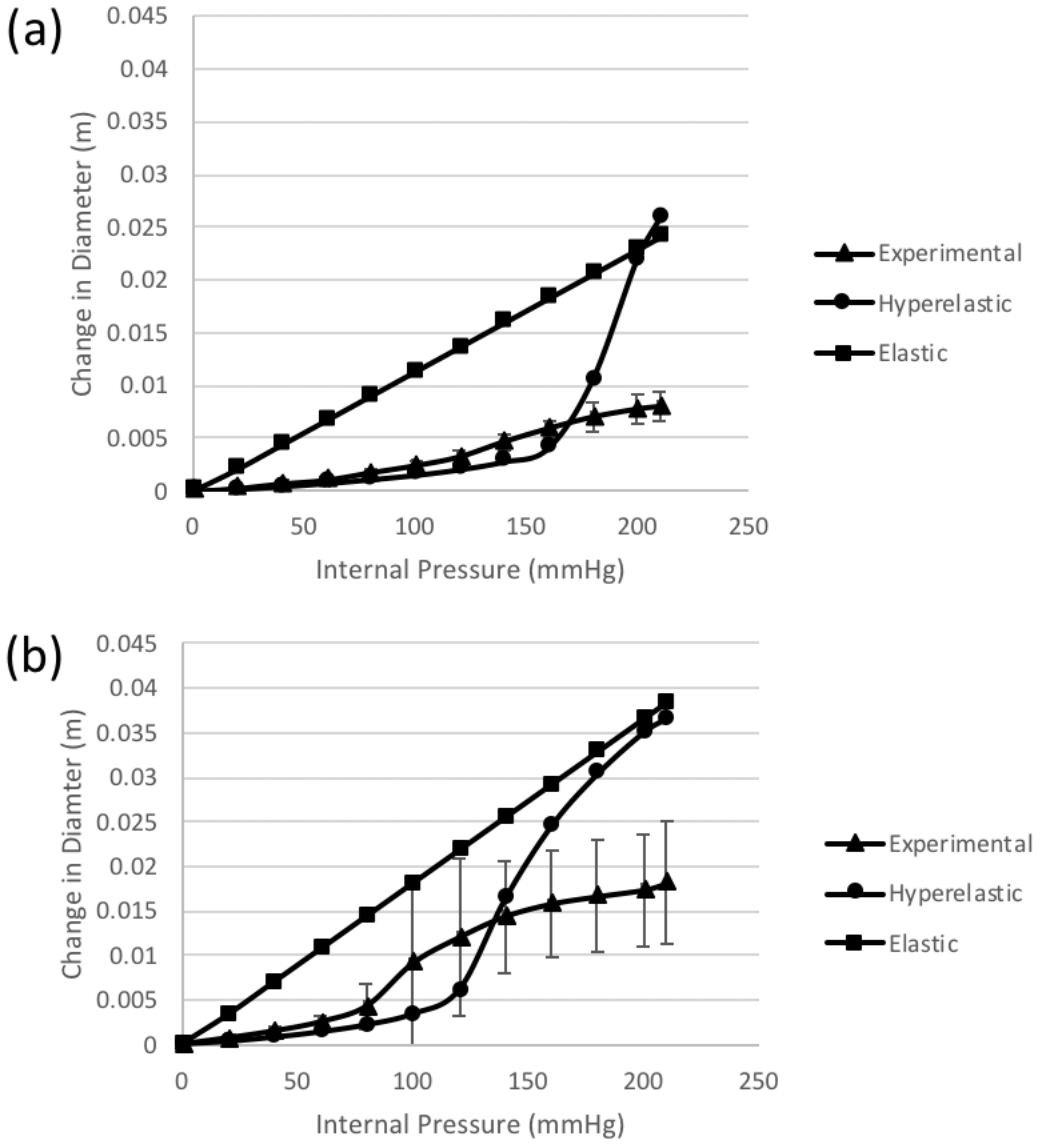


**Figure 4.10 Change in Radius due to applied Internal Pressure.**

The resulting plots of the change in radius vs. internal pressure for (a) uniform wall thickness (b) area of reduced wall thickness illustrate that there is a similar trend experienced between the experimental and hyperelastic results8 not close alignment of the experimental results and either computational model for the full range of pressures experienced in the pressure test. The mean of 3 experimental trials is shown with error bars representing the standard deviation.

However, as discussed in section 3.5 the range we are most interested in is between true strains of 0 and 1.089. This range is of interest as it covers the range of true strain experienced by the average aorta when an AAA develops expanding the aorta gradually from 18.5 mm to 55 mm, at which point intervention for the AAA would be considered. Of the two computational models the hyperelastic model showed the closest correlation. This is consistent with the recommendation made by Simsek and Kwon that hyperelastic computational models provide more realistic results than elastic computational models.[38] Furthermore, the material constants obtained for these computational models were extracted for true strains up to approximately 1.19 mm/mm. The true strains associated with the deformation in the computational model were calculated and recorded in Table 4.4 and the change in radius was plotted again only for strains below 1.089 mm/mm (Fig. 4.11). The resulting plots show a closer agreement, showing similar slopes and inflection points across the range of interest.

**Table 4.4.4 True Strains for Hyperelastic Computational Models**

| | Hyperelastic Material Models | |
|---|---|---|
| | Uniform Wall Thickness | Area of Reduced Wall Thickness |
| Pressure | True Strain | True Strain |
| 0 | 0 | 0 |
| 20 | 0.022848094 | 0.064850972 |
| 40 | 0.050432571 | 0.157763194 |
| 60 | 0.081441216 | 0.264242841 |
| 80 | 0.117980547 | 0.39196701 |
| 100 | 0.157374051 | 0.560631145 |
| 120 | 0.206923831 | 0.855171543 |
| 140 | 0.271383299 | 1.529841401 |
| 160 | 0.372785032 | 1.861682772 |
| 180 | 0.774665722 | 2.046171974 |
| 200 | 1.234986858 | 2.17181813 |
| 210 | 1.352662888 | 2.210835234 |

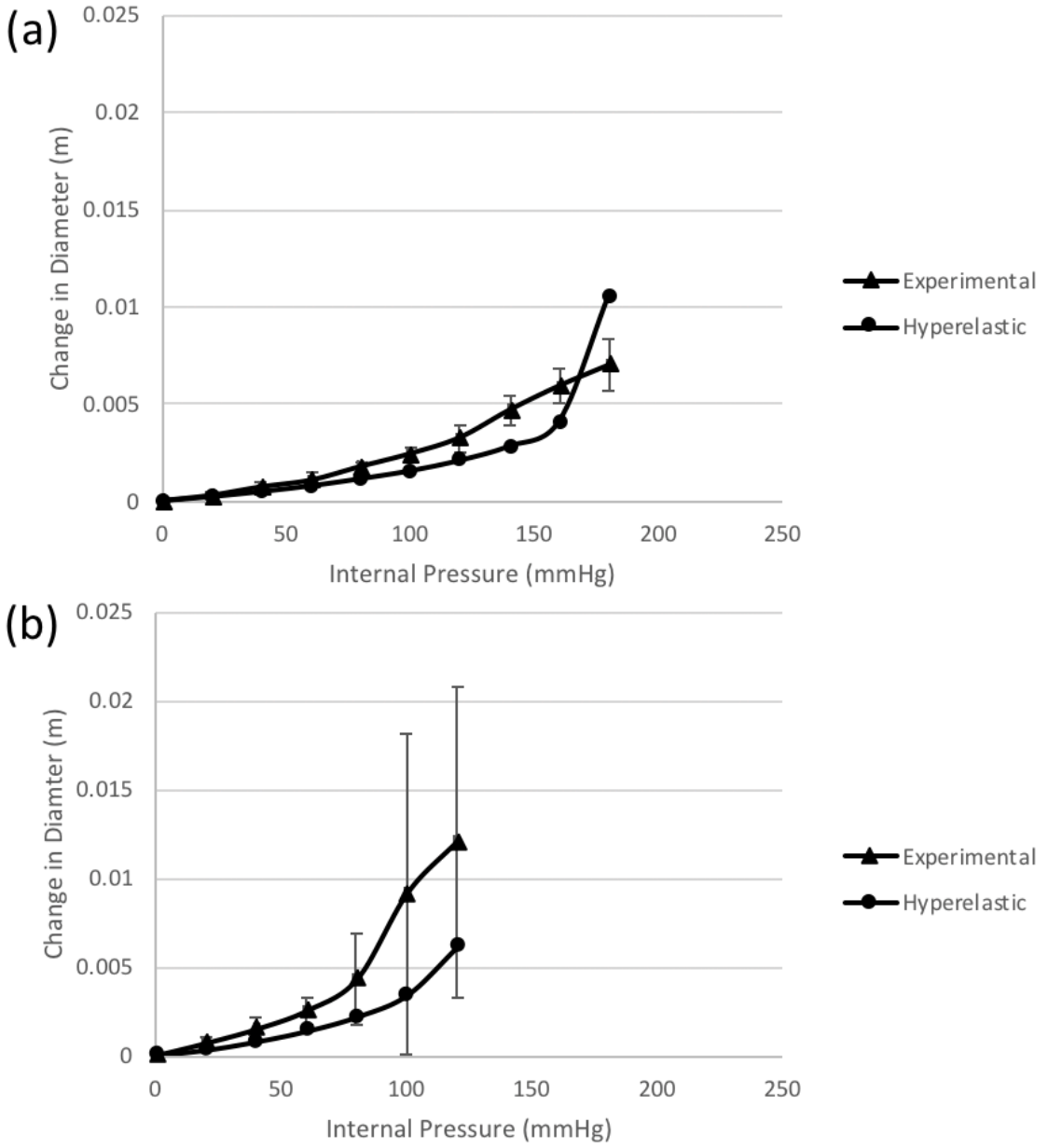


**Figure 4.11 Change in Diameter with Internal Pressure for strains less than 1.089.**

The resulting plots of the change in radius vs. internal pressure for (a) uniform wall thickness (b) area of reduced wall thickness for strains less than 1.089 illustrates that the hyperelastic material model shows a closer agreement, following a similar trend as the experimental model. The mean of 3 experimental trials is shown with error bars representing the standard deviation.

To further investigate if the hyperelastic models captures the trend of model deformation, the change in radius was recorded at 7 points along the length (Fig. 4.12). This was completed for both the experimental model with an area of reduced wall thickness, and the hyperelastic computational model with an area of reduced wall thickness for 3 different pressures; 60mmHg, 80 mmHg, 120 mmHg, and 140 mmHg. The resulting plots (Fig. 4.13) show that the hyperelastic model does depict the trend of deformation along the length experienced during the experiment, however the agreement between the models decreases with the increase in internal pressure.

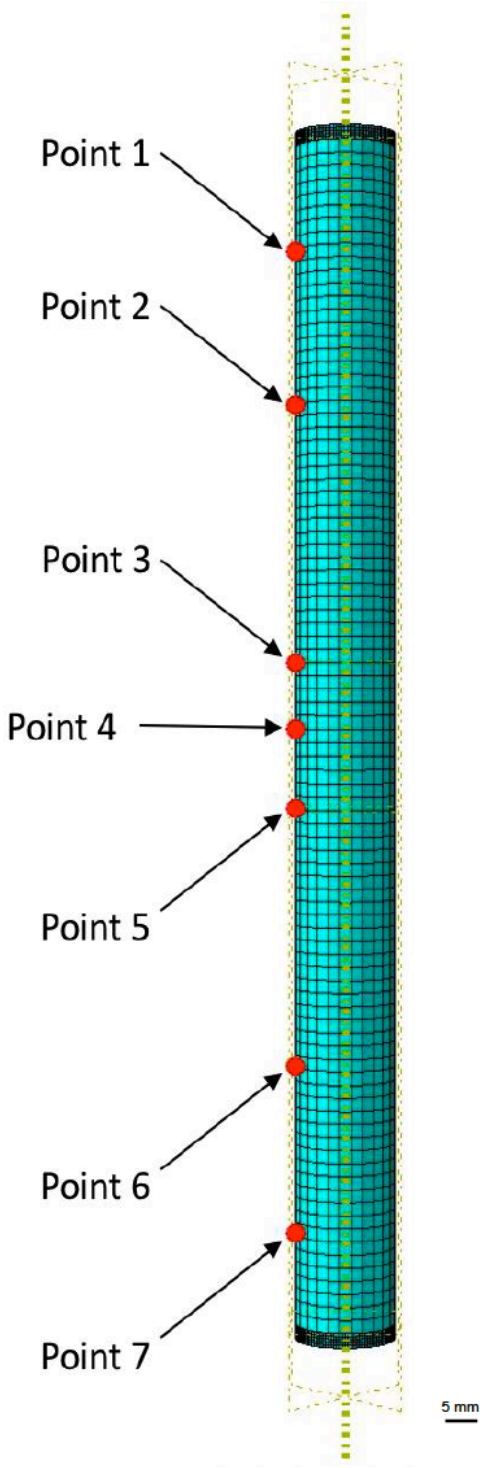


**Figure 4.12 Location along the length where radial deformation was measured.**

The red dots in the image highlight the locations at which the radial deformation was measured along the length of the specimen.

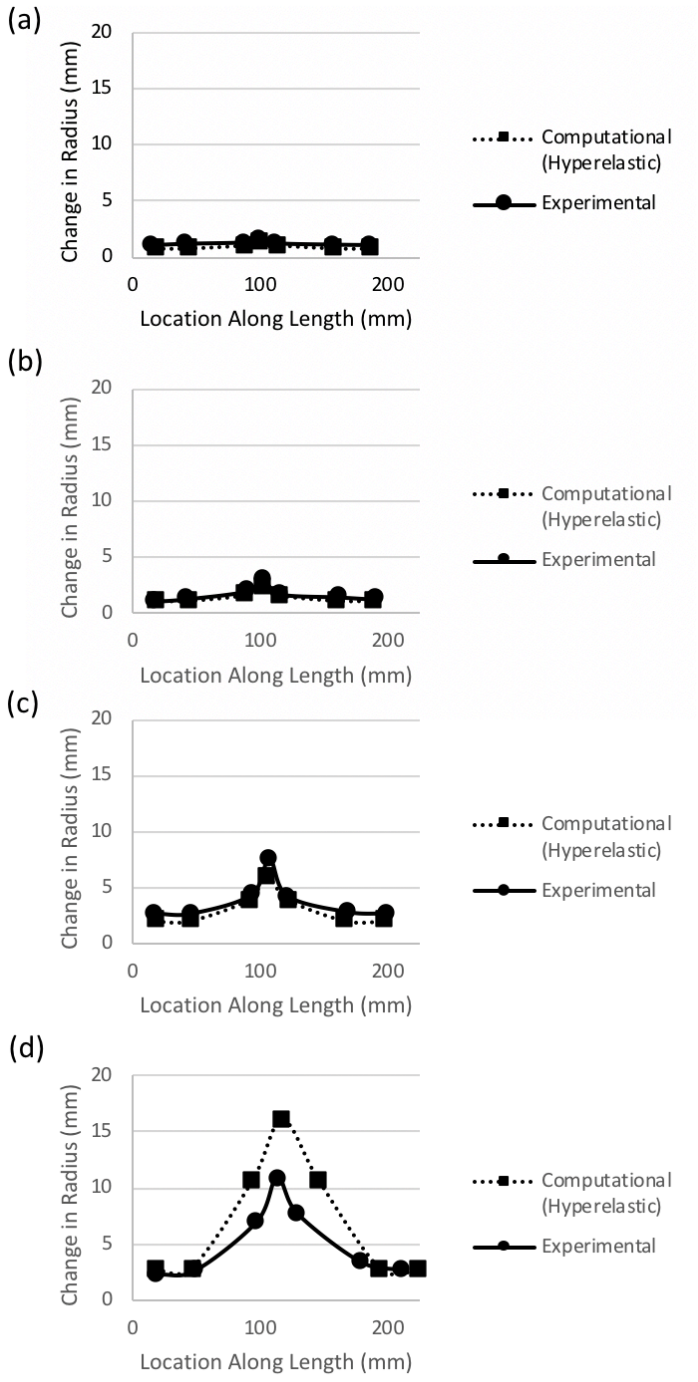


**Figure 4.13 Change in radius along length for both the hyperelastic computational model and experimental models**

The change in radius along the length was recorded at the 7 locations highlights in figure 4.12 for the internal pressures of (a) 60 mmHg (b) 80 mmHg (c) 120 mmHg (d) 140 mmHg. The plots illustrate that the agreement between the computational and experimental model is strong at low internal pressures but weakens as the internal pressure is increased.

Examining figures 4.14 and 4.15 it can be observed that both the computational and experimental tests result in an aneurysmal shape occurring in the models with an area of reduced wall thickness. This provides verification that an area of reduced wall thickness could be a potential trigger for the initiation of abdominal aortic aneurysm formation. When considering that the experimental model is a simplified homogenous model, consisting completely of hyperelastic material, it could be considered that the aorta might see similar results to those observed in this study when there is a reduction in only the medial layer. [15] This could support the theory that diseases, such as atherosclerotic disease, that impact the medial layer could contribute to the development of AAAs. [29]

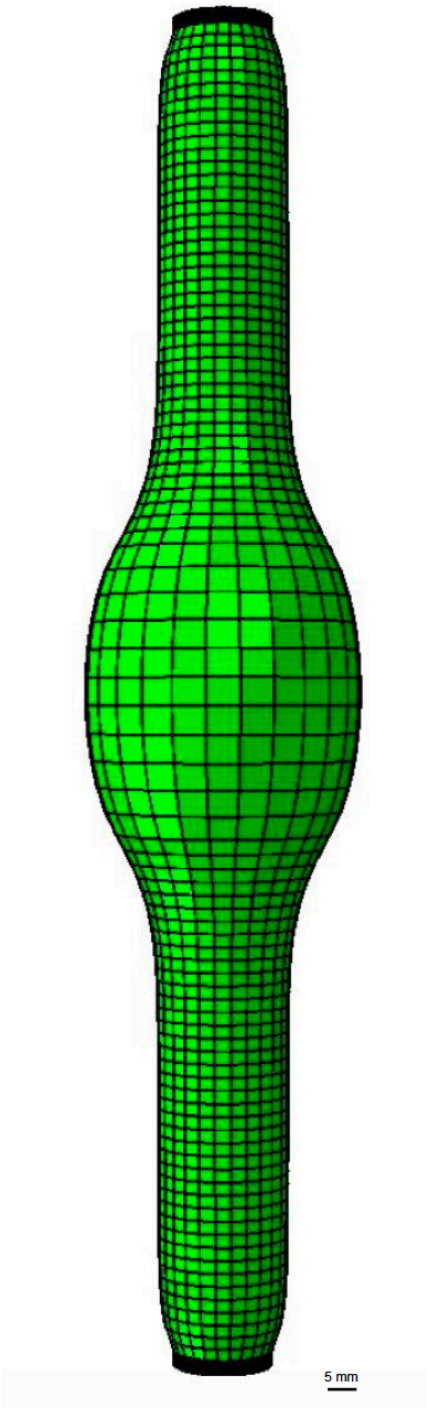


**Figure 4.14 Hyperelastic computational model with area of reduced wall thickness subjected to 140 mmHg.**

When subjected to an internal pressure of 140 mmHg it can be observed that the hyperelastic computational model bulges at the mid region where the wall thickness has been reduced, creating an aneurysmal shape in the specimen.

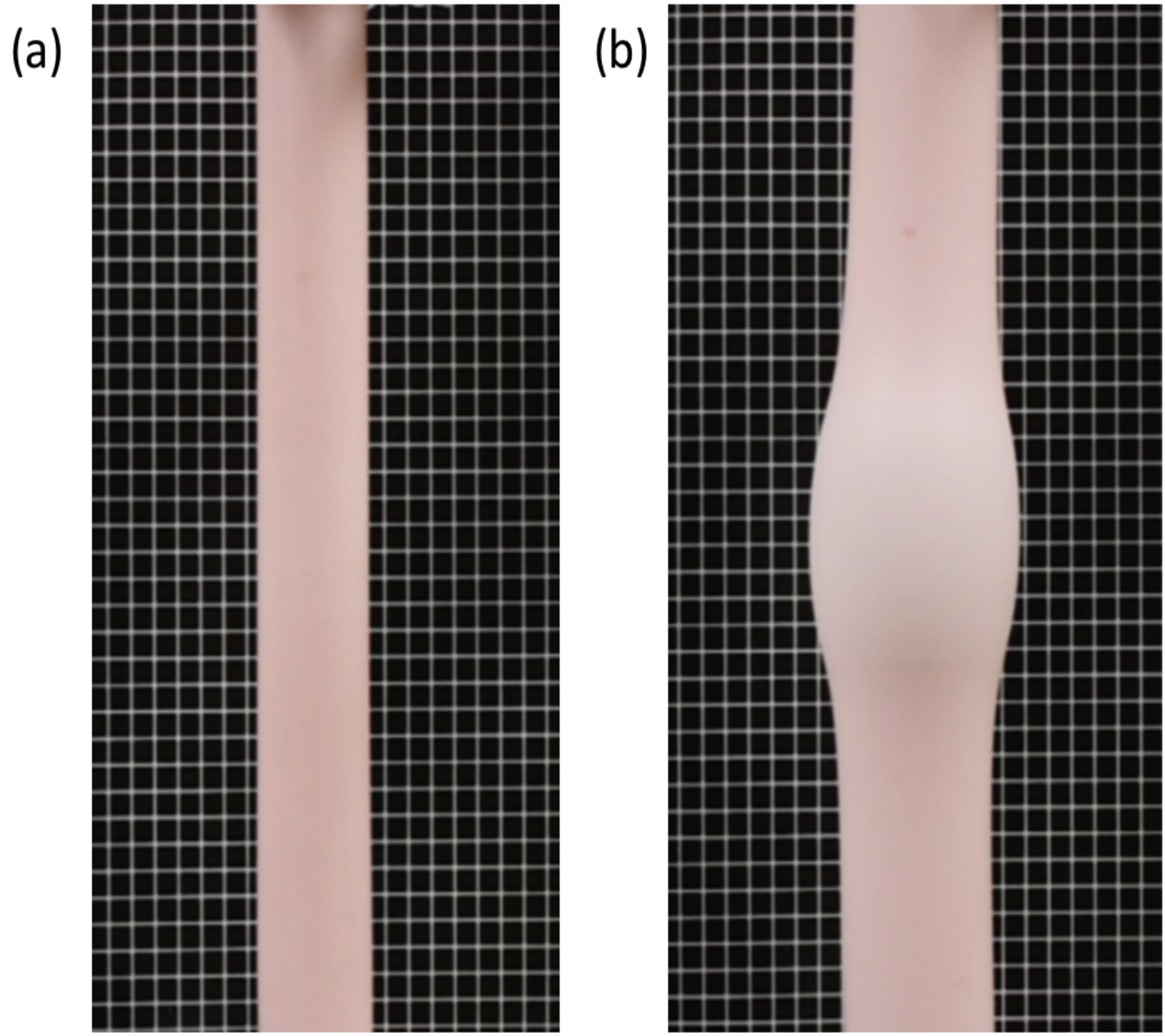


**Figure 4.15 Frame of a pressure test with a reduced wall thickness silicone model at 0 mmHg and 140 mmHg**

As the pressure was increased during the experimental test a bulging area was observed in the region of the tube specimen that has an area of reduced wall thickness, similar to the computational study, creating an aneurysmal shape. This can be observed when comparing the specimen when subjected to 0 mmHg (a), and when subjected to 140 mmHg (b). Grid paper with a 5 mm spacing, visible in the background, was used to quantify diameter changes.

## 4.4 Limitations

There are a number of potential limitations that can be highlighted in this study. First, is the assumption of a simplified material (homogenous, isotropic materials, without irregularities in thickness along the length). This is a simplified approximation when compared to actual aortic tissue. Aortic tissue is known to have multiple fibrous layers with differing axial and circumferential structure [15], which would result in it being nonhomogeneous with anisotropic deformation under pressure.

Second, the effect of viscoelasticity of aortic tissue was not explored in this study. The effect of viscoelasticity could be investigated in future work to see what impact viscoelasticity has on the resulting deformation, and the dynamic deformation across the cardiac cycle. The use of only one material model in the computational testing is another potential limitation. Though a reduced polynomial material model is the most commonly used model when investigating AAAs, it is possible that another model may be more appropriate when considering silicone models. Other SEFs could be considered using the curve fitting function within ABAQUS.

Third, the use of a steady state for analysis. The aorta is subjected to pulsatile fluid flow in vivo. Further research should be conducted to investigate the addition of pulsatile flow to both the in vivo and in vitro models. Ideally these models investigating the effects of pulsatile flow would be completed use a liquid with properties similar to that of human blood. All of these limitations could be addressed individually in future works.

It should also be noted that in a future work, it would be ideal for all these tests to be completed using aortas and aortic tissue with 3D models created to replicate them as closely as possible. However due to the nature of preserving the aortic tissue before testing, the of fresh human aortic samples, and the complexity of customizing 3D models with the exact geometry of each sample it would be a very challenging undertaking. At this point it would be recommended to continuing with simplified models using "tissue-like" materials and increase the complexity gradually.

## 4.5 Conclusions

In this chapter, two investigations were completed in parallel; one computational and one experimental. Two material models were considered for the computational investigation, elastic and hyperelastic. The plots of the change in radius with internal pressure depicted that the hyperelastic model trend was significantly closer to the experimental trend. When considering the change in radius along the length of the specimens at different pressures, for both the hyperelastic and experimental results, it could be observed that the hyperelastic model provided a realistic trend of deformation when considering deformations below the threshold true strain of 1.089. This aligns with the conclusion made by Simsek and Kwon stating that a hyperelastic model would provide a more realistic result than an elastic model when considering AAAs.[38] However, there was still a discrepancy between the experimental and hyperelastic results. The SEF utilized in this study is the most commonly used for AAA simulations. However, when considering silicone, or healthy aortic tissue (pre-aneurysmal) there may be another hyperelastic SEF that more closely aligns with the material behaviour.

Despite the discrepancies between the results of the hyperelastic computational models and experimental models, it could be observed in both models with areas of reduced wall thickness experienced an aneurysmal shape when subjected to internal pressure. As internal pressure was increased, the bulge at the area of reduced wall thickness increased in size, creating a progressively larger aneurysmal shape. This supports the hypothesis that an area of reduced wall thickness, specifically in the medial layer (where the majority of elastin is found) could contribute to the formation of a AAA.

## Chapter 5 : Summary

Very few studies have been completed to date investigating mechanisms of AAA initiation by comparing experimental and computational results. A silicone material was tensile tested, and the elastic and hyperelastic properties were extracted from the stress-strain data produced from the tests. The hyperelastic properties extracted were those corresponding to the most commonly used SEF when studying AAAs, a reduced polynomial.

Computational models with elastic and hyperelastic properties were generated and provided the same material properties as the silicone material that was tensile tested. This same silicone was also used to create experimental silicone models that replicate the computational models. The models were subjected to internal pressure and the resulting change in radius was recorded. The results of these tests highlighted that when considering a material such as silicone, or biological tissue, using a hyperelastic material model for the computational model provides a more realistic result than an elastic material model. This conclusion was support by a previous study that considered elastic and hyperelastic models, but did not compare with an experimental model.[38] Though it could be observed that the hyperelastic material model provided a more realistic trend, there was also discrepancy between the hyperelastic and experimental results. It is possible that the stress-strain behavior of chosen silicone material more closely aligns with another hyperelastic SEF. This could be explored by completing automatic curve fitting within ABAQUS,

then comparing with the experimental results. It is important to use a SEF that provides a realistic result. Completing investigations of the abdominal aorta are challenging in vivo due to their location, and the limits of available imaging technologies. As a result, completing studies computationally is often preferred. It is critical that a computational model that provides an accurate result is used, even when considering simplified approximations for the material as has been done in many previous studies.

Though there was some discrepancy experienced between the hyperelastic computational results and the experimental results, both results illustrated similar deformation trends, showing a bulging area formed when there was an area of reduced wall thickness. As the pressure was increased an obvious aneurysmal shape developed both experimentally and computationally. This supports the hypothesis that an area of reduced wall thickness, or at least a reduction in the medial layer that provides the most elastin to the wall, could be a potential mechanism for AAA initiation. This work provided evidence through experimental testing as well as analytical solution that an area of reduced wall thickness, or thinning of the wall, is a potential cause of AAA initiation. To the best knowledge of the author, this is a novel discovery and not stated or addressed in published literature.

This result could have impacts on the way in which AAAs are monitored and treated. Currently, the standard for intervention of abdominal aortic aneurysms is to monitor the AAA until it reaches a diameter of 5-5.5 cm. However, if the modes of aneurysm initiation were more well established, preventative care could be more closely examined. For example, monitoring programs for pre-aneurysmal indicators in high risk groups could be developed to flag patients who could

be at risk for developing an aneurysm in the near future. Based on the results of this study two potential indicators that could be considered are areas of reduced wall thickness comparative to the rest of the vessel, or signs of atherosclerotic lesions in the medial layer. This monitoring approach may provide insight regarding if, and where, an abdominal aortic aneurysm may form. It would also allow medical teams to determine what, if any, preventative care may be appropriate, and the potential timeline for intervention to reduce the risk of an aneurysm forming. However, it must be acknowledged that these parameters could be challenging to monitor as they would require high quality soft tissue imaging modalities such as MRI to obtain accurate results. As imaging technology advances these parameters may become easier to monitor. These insights could significantly impact the assessment of AAA rupture risk and provide medical teams with quantitative criteria that could inform decisions for early life saving interventions.

**References**


[1] J. Hager, *Abdominal Aortic Aneurysm: Aspects on how to Affect Mortality from Rupture*. Linköping: Linköping University Electronic Press, 2014.

[2] N. Sakalihasan *et al.*, "Abdominal aortic aneurysms," *Nat. Rev. Dis. Prim.*, vol. 4, no. 1, 2018, doi: 10.1038/s41572-018-0030-7.

[3] F. A. Lederle, C. Laine, D. R. Goldmann, and H. C. Sox, "Abdominal aortic aneurysm," *Ann. Intern. Med.*, 2009, doi: 10.1007/BF02597439.

[4] F. A. Lederle, G. R. Johnson, and S. E. Wilson, "Abdominal aortic aneurysm in women," *J. Vasc. Surg.*, vol. 34, no. 1, pp. 122–126, 2001, doi: 10.1067/mva.2001.115275.

[5] F. L. Moll *et al.*, "Management of abdominal aortic aneurysms clinical practice guidelines of the European society for vascular surgery," *Eur. J. Vasc. Endovasc. Surg.*, vol. 41, no. SUPPL. 1, 2011, doi: 10.1016/j.ejvs.2010.09.011.

[6] J. L. Eliason and W. D. Clouse, "Current Management of Infrarenal Abdominal Aortic Aneurysms," *Surg. Clin. North Am.*, vol. 87, no. 5, pp. 1017–1033, 2007, doi: 10.1016/j.suc.2007.08.002.

[7] "Contributor Roles Taxonomy." https://casrai.org/credit/ (accessed Aug. 26, 2021).

[8] M. David and L. Heller, *Cardiovascular Physiology*, 9th ed. McGraw-Hill Education, 2021.

[9] "Blood Flow Through the Heart," *OpenStax College*, 2013.

https://commons.wikimedia.org/wiki/File:2101_Blood_Flow_Through_the_Heart.jpg (accessed Jul. 30, 2023).

[10] J. G. Betts *et al.*, *Anatomy and Physiology*. Houston, Texas: OpenStax, 2013.

[11] D. Chambers, C. Huang, and G. Matthews, "Cardiovascular Physiology," in *Basic Physiology for Anaesthetists*, 2nd ed., Cambridge: Cambridge University Press, 2019, pp. 111–188.

[12] L. Sherwood and C. Ward, *Human Physiology: From Cells to Systems*, 4th ed. Toronto: Nelson Education Ltd, 2019.

[13] "Aorta Anatomy," *University of Florida Health*, 2021. https://ufhealth.org/uf-health-aortic-disease-center/aorta-anatomy.

[14] G. G. Belz, "Elastic properties and Windkessel function of the human aorta," *Cardiovasc. Drugs Ther.*, vol. 9, no. 1, pp. 73–83, 1995, doi: 10.1007/BF00877747.

[15] J. A. Collins, J. V. Munoz, T. R. Patel, M. Loukas, and R. S. Tubbs, "The anatomy of the aging aorta," *Clin. Anat.*, vol. 27, no. 3, pp. 463–466, 2014, doi: 10.1002/ca.22384.

[16] J. A. Niestrawska, P. Regitnig, C. Viertler, T. U. Cohnert, A. R. Babu, and G. A. Holzapfel, "The role of tissue remodeling in mechanics and pathogenesis of abdominal aortic aneurysms," *Acta Biomater.*, vol. 88, pp. 149–161, 2019, doi: 10.1016/j.actbio.2019.01.070.

[17] Edoarado, "Aorta scheme," *Wikimedia Commons*. https://commons.wikimedia.org/wiki/File:Aorta_scheme_noTags.svg#filelinks (accessed Jul. 10, 2023).

[18] J. Golledge and P. E. Norman, "Atherosclerosis and abdominal aortic aneurysm: Cause, response, or common risk factors?," *Arterioscler. Thromb. Vasc. Biol.*, vol. 30, no. 6, pp.

1075–1077, 2010, doi: 10.1161/ATVBAHA.110.206573.

[19] J. Cornuz, C. S. Pinto, H. Tevaearai, and M. Egger, "Risk factors for asymptomatic abdominal aortic aneurysm: Sytematic review and meta-analysis of population-based screening studies," *Eur. J. Public Health*, vol. 14, no. 4, pp. 343–349, 2004, doi: 10.1093/eurpub/14.4.343.

[20] B. G. DeRubertis *et al.*, "Abdominal aortic aneurysm in women: Prevalence, risk factors, and implications for screening," *J. Vasc. Surg.*, vol. 46, no. 4, pp. 16–20, 2007, doi: 10.1016/j.jvs.2007.06.024.

[21] D. C. Brewster, J. L. Cronenwett, J. W. Hallett, K. W. Johnston, W. C. Krupski, and J. S. Matsumura, "Guidelines for the treatment of abdominal aortic aneurysms: Report of a subcommittee of the Joint Council of the American Association for Vascular Surgery and Society for Vascular Surgery," *J. Vasc. Surg.*, vol. 37, no. 5, pp. 1106–1117, 2003, doi: 10.1067/mva.2003.363.

[22] G. Dangas *et al.*, "Open versus endovascular stent graft repair of abdominal aortic aneurysms: A meta-analysis of randomized trials," *JACC Cardiovasc. Interv.*, vol. 5, no. 10, pp. 1071–1080, 2012, doi: 10.1016/j.jcin.2012.06.015.

[23] F. A. Lederle, R. L. Kane, R. MacDonald, and T. J. Wilt, "Systematic review: Repair of unruptured abdominal aortic aneurysm," *Ann. Intern. Med.*, vol. 146, no. 10, pp. 735–741, 2007, doi: 10.7326/0003-4819-146-10-200705150-00007.

[24] Jakob Hager, *Abdominal Aortic Aneurysm*. Linköping: Linköping University Electronic Press, 2014.

[25] D. C. Iliopoulos, E. P. Kritharis, A. T. Giagini, S. A. Papadodima, and D. P. Sokolis, "Ascending thoracic aortic aneurysms are associated with compositional remodeling and

vessel stiffening but not weakening in age-matched subjects," *J. Thorac. Cardiovasc. Surg.*, vol. 137, no. 1, pp. 101–109, 2009, doi: 10.1016/j.jtcvs.2008.07.023.

[26] M. L. Raghavan, J. Kratzberg, E. M. Castro de Tolosa, M. M. Hanaoka, P. Walker, and E. S. da Silva, "Regional distribution of wall thickness and failure properties of human abdominal aortic aneurysm," *J. Biomech.*, vol. 39, no. 16, pp. 3010–3016, 2006, doi: 10.1016/j.jbiomech.2005.10.021.

[27] A. J. Lusis, "Atherosclerosis - Insight Review Articles," *Nature*, vol. 407, no. September, pp. 233–241, 2000, [Online]. Available: http://www.pubmedcentral.nih.gov/articlerender.fcgi?artid=2826222&tool=pmcentrez&rendertype=abstract.

[28] G. Candore *et al.*, "Atherosclerosis," *Cytokine Gene Polymorphisms Multifactorial Cond.*, vol. 104, pp. 363–378, 2006, doi: 10.29309/tpmj/2017.24.10.717.

[29] T. M. McGloughlin, *Biomechanics and Mechanobiology of Aneurysms*. 2011.

[30] A. C. van der Wal, A. E. Becker, and P. K. Das, "Medial thinning and atherosclerosis - evidence for involvement of a local inflammatory effect," *Atherosclerosis*, vol. 103, no. 1, pp. 55–64, 1993, doi: 10.1016/0021-9150(93)90039-W.

[31] J. F. Bentzon, G. Pasterkamp, and E. Falk, "Expansive remodeling is a response of the plaque-related vessel wall in aortic roots of apoE-deficient mice: An experiment of nature," *Arterioscler. Thromb. Vasc. Biol.*, vol. 23, no. 2, pp. 257–262, 2003, doi: 10.1161/01.ATV.0000051387.70962.79.

[32] M. F. O. Rourke, "Pulsatile arterial haefiodynamics i n hypertension," vol. 6, pp. 40–48, 2010.

[33] C. Hillery, "Mechanical and morphological characterisitics of elastin from conduit

arteries," Queen Mary College, University of London, 2005.

[34] D. A. Vorp, "Biomechanics of abdominal aortic aneurysm," *J. Biomech.*, vol. 40, no. 9, pp. 1887–1902, 2007, doi: 10.1016/j.jbiomech.2006.09.003.

[35] E. S. Di Martino, A. Bohra, J. P. Vande Geest, N. Gupta, M. S. Makaroun, and D. A. Vorp, "Biomechanical properties of ruptured versus electively repaired abdominal aortic aneurysm wall tissue," *J. Vasc. Surg.*, vol. 43, no. 3, pp. 570–576, 2006, doi: 10.1016/j.jvs.2005.10.072.

[36] V. A. Korshunov, S. M. Schwartz, and B. C. Berk, "Vascular remodeling: Hemodynamic and biochemical mechanisms underlying Glagov's phenomenon," *Arterioscler. Thromb. Vasc. Biol.*, vol. 27, no. 8, pp. 1722–1728, 2007, doi: 10.1161/ATVBAHA.106.129254.

[37] E. G. Lakatta, J. H. Mitchell, A. Pomerance, and G. G. Rowe, "Human aging: Changes in structure and function," *J. Am. Coll. Cardiol.*, vol. 10, no. 2, pp. 42A-47A, 1987, doi: 10.1016/S0735-1097(87)80447-3.

[38] F. G. Simsek and Y. W. Kwon, "Investigation of material modeling in fluid–structure interaction analysis of an idealized three-layered abdominal aorta: aneurysm initiation and fully developed aneurysms," *J. Biol. Phys.*, vol. 41, no. 2, pp. 173–201, 2015, doi: 10.1007/s10867-014-9372-x.

[39] J. Birjiniuk *et al.*, "Development and testing of a silicone in vitro model of descending aortic dissection," *J. Surg. Res.*, vol. 198, no. 2, pp. 502–507, 2015, doi: 10.1016/j.jss.2015.03.024.

[40] A. Hossien, "Comprehensive middle-fidelity simulator for training in aortic root surgery," *J. Surg. Educ.*, vol. 72, no. 5, pp. 849–854, 2015, doi: 10.1016/j.jsurg.2015.04.024.

[41] L. Morris, P. O'Donnell, P. Delassus, and T. McGloughlin, "Experimental assessment of

stress patterns in abdominal aortic aneurysms using the photoelastic method," *Strain*, vol. 40, no. 4, pp. 165–172, 2004, doi: 10.1111/j.1475-1305.2004.tb01425.x.

[42] M. Russo *et al.*, "Advanced three-dimensionally engineered simulation model for aortic valve and proximal aorta procedures," *Interact. Cardiovasc. Thorac. Surg.*, vol. 30, no. 6, pp. 887–895, 2020, doi: 10.1093/ICVTS/IVAA026.

[43] J. L. Sparks *et al.*, "Use of silicone materials to simulate tissue biomechanics as related to deep tissue injury," *Adv. Ski. Wound Care*, vol. 28, no. 2, pp. 59–68, 2015, doi: 10.1097/01.ASW.0000460127.47415.6e.

[44] P. Bihari *et al.*, "Strain measurement of abdominal aortic aneurysm with real-time 3D ultrasound speckle tracking," *Eur. J. Vasc. Endovasc. Surg.*, vol. 45, no. 4, pp. 315–323, 2013, doi: 10.1016/j.ejvs.2013.01.004.

[45] B. J. Doyle *et al.*, "Experimental modelling of aortic aneurysms: Novel applications of silicone rubbers," *Med. Eng. Phys.*, vol. 31, no. 8, pp. 1002–1012, 2009, doi: 10.1016/j.medengphy.2009.06.002.

[46] T. J. Corbett, B. J. Doyle, A. Callanan, M. T. Walsh, and T. M. McGloughlin, "Engineering silicone rubbers for in vitro studies: Creating AAA models and ILT analogues with physiological properties," *J. Biomech. Eng.*, vol. 132, no. 1, pp. 1–9, 2010, doi: 10.1115/1.4000156.

[47] B. J. Doyle, A. J. Cloonan, M. T. Walsh, D. A. Vorp, and T. M. McGloughlin, "Identification of rupture locations in patient-specific abdominal aortic aneurysms using experimental and computational techniques," *J. Biomech.*, vol. 43, no. 7, pp. 1408–1416, 2010, doi: 10.1016/j.jbiomech.2009.09.057.

[48] S. Marconi *et al.*, "A compliant aortic model for in vitro simulations: Design and

manufacturing process," *Med. Eng. Phys.*, vol. 59, pp. 21–29, 2018, doi: 10.1016/j.medengphy.2018.04.022.

[49] B. J. Doyle, L. G. Morris, A. Callanan, P. Kelly, D. A. Vorp, and T. M. McGloughlin, "3D reconstruction and manufacture of real abdominal aortic aneurysms: From CT scan to silicone model," *J. Biomech. Eng.*, vol. 130, no. 3, 2008, doi: 10.1115/1.2907765.

[50] M. L. Raghavan and D. A. Vorp, "Toward a biomechanical tool to evaluate rupture potential of abdominal aortic aneurysm: Identification of a finite strain constitutive model and evaluation of its applicability," *J. Biomech.*, vol. 33, no. 4, pp. 475–482, 2000, doi: 10.1016/S0021-9290(99)00201-8.

[51] J. B. Choi *et al.*, "Pressure distribution and wall shear stress in stenosis and abdominal aortic aneurysm by computational fluid dynamics modeling (CFD)," *Korean J. Chem. Eng.*, vol. 31, no. 3, pp. 402–411, 2014, doi: 10.1007/s11814-013-0215-4.

[52] S. Patel, A. Y. Usmani, and K. Muralidhar, "Effect of aorto-iliac bifurcation and iliac stenosis on flow dynamics in an abdominal aortic aneurysm," *Fluid Dyn. Res.*, vol. 49, no. 3, 2017, doi: 10.1088/1873-7005/aa6a6b.

[53] Y. H. Lu, K. Mani, B. Panigrahi, W. T. Hsu, and C. Y. Chen, "Endoleak Assessment Using Computational Fluid Dynamics and Image Processing Methods in Stented Abdominal Aortic Aneurysm Models," *Comput. Math. Methods Med.*, vol. 2016, 2016, doi: 10.1155/2016/9567294.

[54] T. Frauenfelder, M. Lotfey, T. Boehm, and S. Wildermuth, "Computational fluid dynamics: Hemodynamic changes in abdominal aortic aneurysm after stent-graft implantation," *Cardiovasc. Intervent. Radiol.*, vol. 29, no. 4, pp. 613–623, 2006, doi: 10.1007/s00270-005-0227-5.

[55] B. A. Howell, T. Kim, A. Cheer, H. Dwyer, D. Saloner, and T. A. M. Chuter, "Computational fluid dynamics within bifurcated abdominal aortic stent-grafts," *J. Endovasc. Ther.*, vol. 14, no. 2, pp. 138–143, 2007, doi: 10.1583/1545-1550(2007)14[138:CFDWBA]2.0.CO;2.

[56] T. P. Nghiem, R. Moreno, M. H. Tran, A. N. Salvayre, and H. Rousseau, "Computational Fluid Dynamics: Morphological and Hemodynamic Changes in Abdominal Aortic Aneurysm," *J. Am. Coll. Cardiol.*, vol. 63, no. 12, p. A1213, 2014, doi: 10.1016/s0735-1097(14)61213-4.

[57] J. E. Moore, "Re: Analytical Modeling and Numerical Simulation of Forces in an Endoluminal Graft," *J. Endovasc. Ther.*, vol. 9, no. 2, pp. 251–252, 2002, doi: 10.1177/152660280200900222.

[58] P. Erhart *et al.*, "Finite element analysis in asymptomatic, symptomatic, and ruptured abdominal aortic aneurysms: In search of new rupture risk predictors," *Eur. J. Vasc. Endovasc. Surg.*, vol. 49, no. 3, pp. 239–245, 2015, doi: 10.1016/j.ejvs.2014.11.010.

[59] T. C. Gasser, M. Auer, F. Labruto, J. Swedenborg, and J. Roy, "Biomechanical rupture risk assessment of abdominal aortic aneurysms: Model complexity versus predictability of finite element simulations," *Eur. J. Vasc. Endovasc. Surg.*, vol. 40, no. 2, pp. 176–185, 2010, doi: 10.1016/j.ejvs.2010.04.003.

[60] D. Azar, D. Ohadi, A. Rachev, J. F. Eberth, M. J. Uline, and T. Shazly, "Mechanical and geometrical determinants of wall stress in abdominal aortic aneurysms: A computational study," *PLoS One*, vol. 13, no. 2, pp. 1–15, 2018, doi: 10.1371/journal.pone.0192032.

[61] T. C. Gasser, M. Auer, F. Labruto, J. Swedenborg, and J. Roy, "Biomechanical rupture risk assessment of abdominal aortic aneurysms: Model complexity versus predictability of

finite element simulations," *Eur. J. Vasc. Endovasc. Surg.*, vol. 40, no. 2, pp. 176–185, 2010, doi: 10.1016/j.ejvs.2010.04.003.

[62] A. Hyhlik-Dürr, T. Krieger, P. Geisbüsch, D. Kotelis, T. Able, and D. Böckler, "Reproducibility of deriving parameters of AAA rupture risk from patient-specific 3D finite element models," *J. Endovasc. Ther.*, vol. 18, no. 3, pp. 289–298, 2011, doi: 10.1583/10-3384MR.1.

[63] G. Martufi, A. Satriano, R. D. Moore, D. A. Vorp, and E. S. Di Martino, "Local Quantification of Wall Thickness and Intraluminal Thrombus Offer Insight into the Mechanical Properties of the Aneurysmal Aorta," *Ann. Biomed. Eng.*, vol. 43, no. 8, pp. 1759–1771, 2015, doi: 10.1007/s10439-014-1222-2.

[64] B. J. Doyle, A. Callanan, M. T. Walsh, P. A. Grace, and T. M. McGloughlin, "A Finite Element Analysis Rupture Index (FEARI) as an Additional Tool for Abdominal Aortic Aneurysm Rupture Prediction," *Vasc. Dis. Prev.*, vol. 6, no. 1, pp. 114–121, 2009, doi: 10.2174/1567270000906010114.

[65] A. K. Venkatasubramaniam *et al.*, "A comparative study of aortic wall stress using finite element analysis for ruptured and non-ruptured abdominal aortic aneurysms," *Eur. J. Vasc. Endovasc. Surg.*, vol. 28, no. 2, pp. 168–176, 2004, doi: 10.1016/j.ejvs.2004.03.029.

[66] L. Speelman *et al.*, "Patient-Specific AAA Wall Stress Analysis: 99-Percentile Versus Peak Stress," *Eur. J. Vasc. Endovasc. Surg.*, vol. 36, no. 6, pp. 668–676, 2008, doi: 10.1016/j.ejvs.2008.09.007.

[67] L. Speelman *et al.*, "The Influence of Wall Stress on AAA Growth and Biomarkers," *Eur. J. Vasc. Endovasc. Surg.*, vol. 39, no. 4, pp. 410–416, 2010, doi: 10.1016/j.ejvs.2009.12.021.

[68] B. J. B. M. Wolters, M. C. M. Rutten, G. W. H. Schurink, U. Kose, J. De Hart, and F. N. Van De Vosse, "A patient-specific computational model of fluid-structure interaction in abdominal aortic aneurysms," *Med. Eng. Phys.*, vol. 27, no. 10, pp. 871–883, 2005, doi: 10.1016/j.medengphy.2005.06.008.

[69] M. Xenos *et al.*, "Patient-based abdominal aortic aneurysm rupture risk prediction with fluid structure interaction modeling," *Ann. Biomed. Eng.*, vol. 38, no. 11, pp. 3323–3337, 2010, doi: 10.1007/s10439-010-0094-3.

[70] E. A. Finol, E. S. Di Martino, D. a. Vorp, and C. H. Amon, "Fluid-Structure Interaction and Structural Analyses of an Aneurysm Model," *N. Engl. J. Med.*, vol. 339, no. 24, pp. 1725–1733, 1998, [Online]. Available: http://www.nejm.org/doi/abs/10.1056/NEJM199812103392401.

[71] C. M. Scotti and E. A. Finol, "Compliant biomechanics of abdominal aortic aneurysms: A fluid-structure interaction study," *Comput. Struct.*, vol. 85, no. 11–14, pp. 1097–1113, 2007, doi: 10.1016/j.compstruc.2006.08.041.

[72] J. H. Leung *et al.*, "Fluid structure interaction of patient specific abdominal aortic aneurisms: A comparison with solid stress models," *Biomed. Eng. Online*, vol. 5, pp. 1–15, 2006, doi: 10.1186/1475-925X-5-33.

[73] M. Xenos *et al.*, "Progression of Abdominal Aortic Aneurysm Towards Rupture: Refining Clinical Risk Assessment Using a Fully Coupled Fluid–Structure Interaction Method," *Ann. Biomed. Eng.*, vol. 43, no. 1, pp. 139–153, 2015, doi: 10.1007/s10439-014-1224-0.

[74] D. S. Molony, A. Callanan, E. G. Kavanagh, M. T. Walsh, and T. M. McGloughlin, "Fluid-structure interaction of a patient-specific abdominal aortic aneurysm treated with an endovascular stent-graft.," *Biomed. Eng. Online*, vol. 8, p. 24, 2009, doi:

10.1186/1475-925X-8-24.

[75] E. S. Di Martino *et al.*, "Fluid-structure interaction within realistic three-dimensional models of the aneurysmatic aorta as a guidance to assess the risk of rupture of the aneurysm," *Med. Eng. Phys.*, vol. 23, no. 9, pp. 647–655, 2001, doi: 10.1016/S1350-4533(01)00093-5.

[76] C. M. Scotti, A. D. Shkolnik, S. C. Muluk, and E. A. Finol, "Fluid-structure interaction in abdominal aortic aneurysms: Effects of asymmetry and wall thickness," *Biomed. Eng. Online*, vol. 4, pp. 1–22, 2005, doi: 10.1186/1475-925X-4-64.

[77] D. A. Vorp, M. L. Raghavan, and M. W. Webster, "Mechanical wall stress in abdominal aortic aneurysm: Influence of diameter and asymmetry," *J. Vasc. Surg.*, vol. 27, no. 4, pp. 632–639, 1998, doi: 10.1016/S0741-5214(98)70227-7.

[78] C. Kleinstreuer, Z. Li, and M. A. Farber, "Fluid-structure interaction analyses of stented abdominal aortic aneurysms," *Annu. Rev. Biomed. Eng.*, vol. 9, pp. 169–204, 2007, doi: 10.1146/annurev.bioeng.9.060906.151853.

[79] M. L. Raghavan, M. W. Webster, and D. A. Vorp, "Ex vivo biomechanical behavior of abdominal aortic aneurysm: Assessment using a new mathematical model," *Ann. Biomed. Eng.*, vol. 24, no. 5, pp. 573–582, 1996, doi: 10.1007/bf02684226.

[80] A. Maier, M. W. Gee, C. Reeps, H. H. Eckstein, and W. A. Wall, "Impact of calcifications on patient-specific wall stress analysis of abdominal aortic aneurysms," *Biomech. Model. Mechanobiol.*, vol. 9, no. 5, pp. 511–521, 2010, doi: 10.1007/s10237-010-0191-0.

[81] B. J. Doyle *et al.*, "Vessel asymmetry as an additional diagnostic tool in the assessment of abdominal aortic aneurysms," *J. Vasc. Surg.*, vol. 49, no. 2, pp. 443–454, 2009, doi: 10.1016/j.jvs.2008.08.064.

[82] G. Ziervogel *et al.*, "Climate change and adaptation in African agriculture," *Training*, vol. 4179, no. October 2012, p. 53, 2008, doi: 10.1002/cnm.

[83] M. L. Raghavan, D. A. Vorp, M. P. Federle, M. S. Makaroun, and M. W. Webster, "Wall stress distribution on three-dimensionally reconstructed models of human abdominal aortic aneurysm," *J. Vasc. Surg.*, vol. 31, no. 4, pp. 760–769, 2000, doi: 10.1067/mva.2000.103971.

[84] D. H. J. Wang, M. S. Makaroun, M. W. Webster, and D. A. Vorp, "Effect of intraluminal thrombus on wall stress in patient-specific models of abdominal aortic aneurysm," *J. Vasc. Surg.*, vol. 36, no. 3, pp. 598–604, 2002, doi: 10.1067/mva.2002.126087.

[85] M. F. Fillinger, M. L. Raghavan, S. P. Marra, J. L. Cronenwett, and F. E. Kennedy, "In vivo analysis of mechanical wall stress and abdominal aortic aneurysm rupture risk," *J. Vasc. Surg.*, vol. 36, no. 3, pp. 589–597, 2002, doi: 10.1067/mva.2002.125478.

[86] Smooth-On, "Smooth-Sil ™ Series." https://www.smooth-on.com/tb/files/SMOOTH-SIL_SERIES_TB.pdf.

[87] S. H. Teoh, Z. G. Tang, and G. W. Hastings, *Handbook of Biomaterial Properties, Second Edition*, 2nd ed. New York: Springer Nature, 2016.

[88] A. D412-16(2021), *Standard Test Methods for Vulcanized Rubber and Thermoplastic Elastomers—Tension*. West Conshohocken, PA: ASTM International, 2021.

[89] J. Gere and B. Goodno, *Mechanics of Materials*. Stamford: Cengage.

[90] A. Rohatgi, "WebPlotDigitizer." https://automeris.io/WebPlotDigitizer (accessed Jan. 10, 2021).

[91] A. Maier, M. W. Gee, C. Reeps, J. Pongratz, H. H. Eckstein, and W. A. Wall, "A comparison of diameter, wall stress, and rupture potential index for abdominal aortic

aneurysm rupture risk prediction," *Ann. Biomed. Eng.*, vol. 38, no. 10, pp. 3124–3134, 2010, doi: 10.1007/s10439-010-0067-6.

[92] E. G. O'Hara, "Mechanical Properties of Silicone Rubber in a Closed Volume," 1983.

[93] FARO, "FARO Laser ScanArm ® V2." https://downloads.faro.com/index.php/s/WwTpTbzfGaQaPS5.

[94] R. Akhtar, M. J. Sherratt, J. K. Cruickshank, and B. Derby, "Characterizing the elastic properties of tissues," *Mater. Today*, vol. 14, no. 3, pp. 96–105, 2011, doi: 10.1016/S1369-7021(11)70059-1.

[95] W. Halpern, G. Osol, and G. S. Coy, "Mechanical behavior of pressurized in vitro prearteriolar vessels determined with a video system," *Ann. Biomed. Eng.*, vol. 12, no. 5, pp. 463–479, 1984, doi: 10.1007/BF02363917.

[96] A. Quotb, E. E. Ramírez-Miquet, C. Tronche, and J. Perchoux, "Optical Feedback Interferometry sensor for flow characterization inside ex-vivo vessel," *Proc. IEEE Sensors*, vol. 2014-Decem, no. December, pp. 362–365, 2014, doi: 10.1109/ICSENS.2014.6985009.